ACTINIDE TRANSFER IN-SITU OF GEOLOGICAL FORMATIONS: MINERAL-CHEMICAL AND ISOTOPE-GEOCHEMICAL ASPECTS

Vladislav A. Petrov

Institute of Geology of Ore Deposits, Petrography, Mineralogy and Geochemistry (IGEM)
Russian Academy of Sciences, Moscow, Russia

vlad243@igem.ru

Joint ICTP-IAEA International School on Nuclear Waste Actinide Immobilization

Trieste, Italy, 10-14 September 2018

Main aspects of radionuclide transport processes

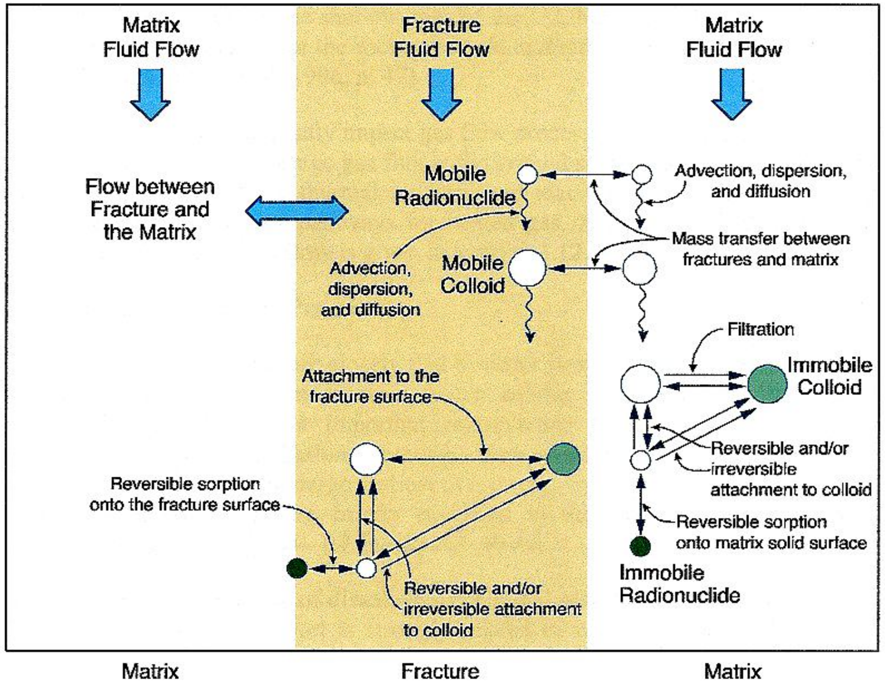

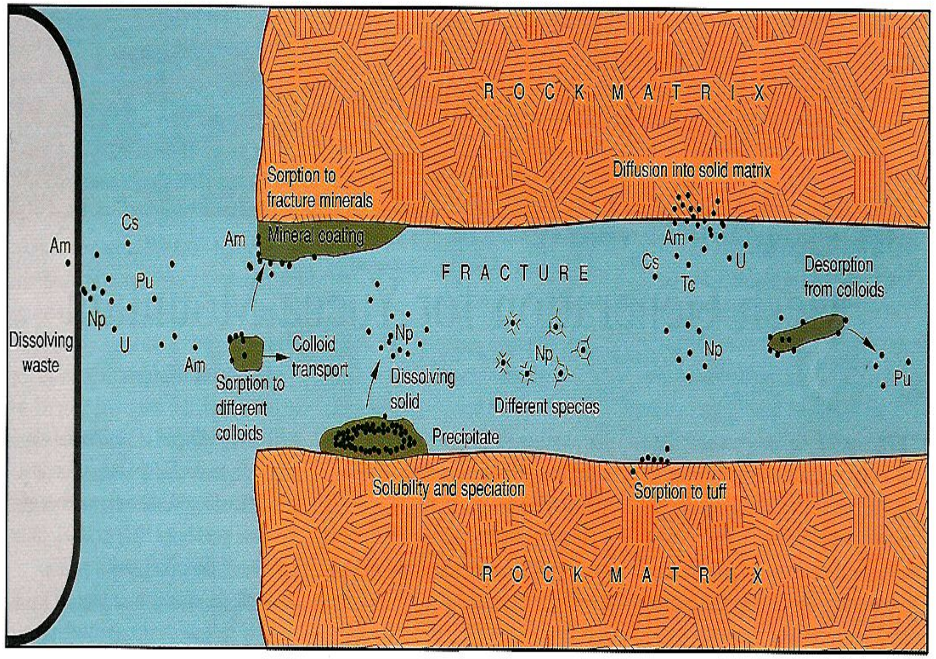

(a) Important radionuclide transport processes (after *Bodvarsson et al., 2000*).
Note that the radionuclides also undergo radioactive decay, but this is not shown in the scheme.

(b) Geochemical factors for radionuclide transport (after *Eckhardt, 2000*) in the context of RW disposal.
This depiction of breached waste canister shows escaping of dissolved radionuclides from the repository through water-filled rock fractures and their impeding by the surrounding rock matrix. These data are important for defining the chemical and physical parameters for modeling.

Mechanisms of migration of radionuclides and colloids through hydraulically active fracture – near fracture space

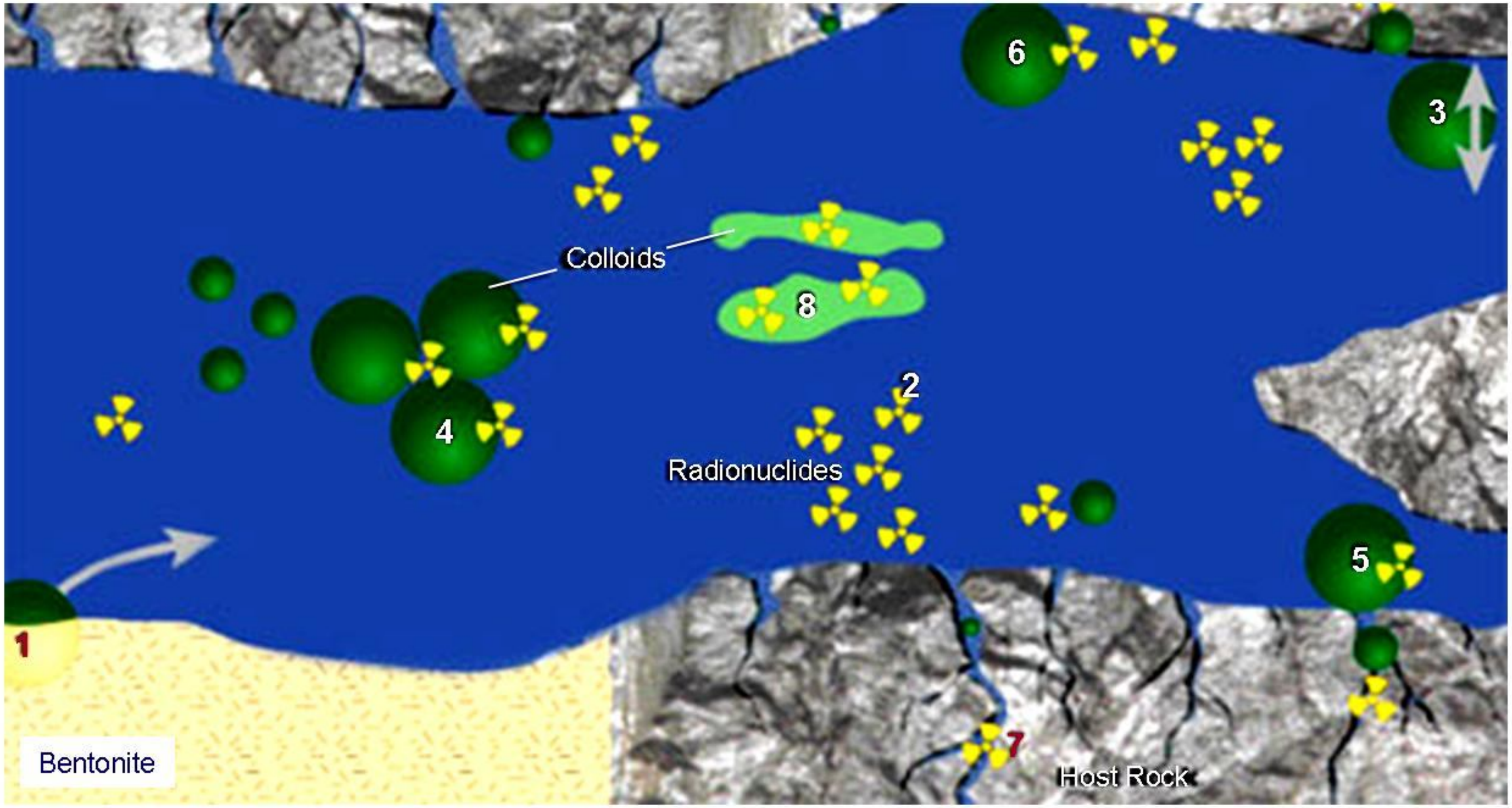

Main mechanisms of migration of radionuclides and colloids are: *1*) Formation of inorganic colloids; *2*) Dissolution of radionuclides in water; *3*) Sorption / desorption of colloids on the fracture surface; *4*) Sorption of radionuclides by inorganic colloids; *5*) Filtration of colloids; *6*) Dimensions of colloids determine their penetration into the rock matrix pore space; *7*) Diffusion of radionuclides into the rock matrix pore space; *8*) Sorption and incorporation of radionuclides by organic colloids (*after NAGRA, 2001*).

Some mechanisms of radionuclide migration which affect on distribution coefficient (K_d) and retardation factor (R_f) values

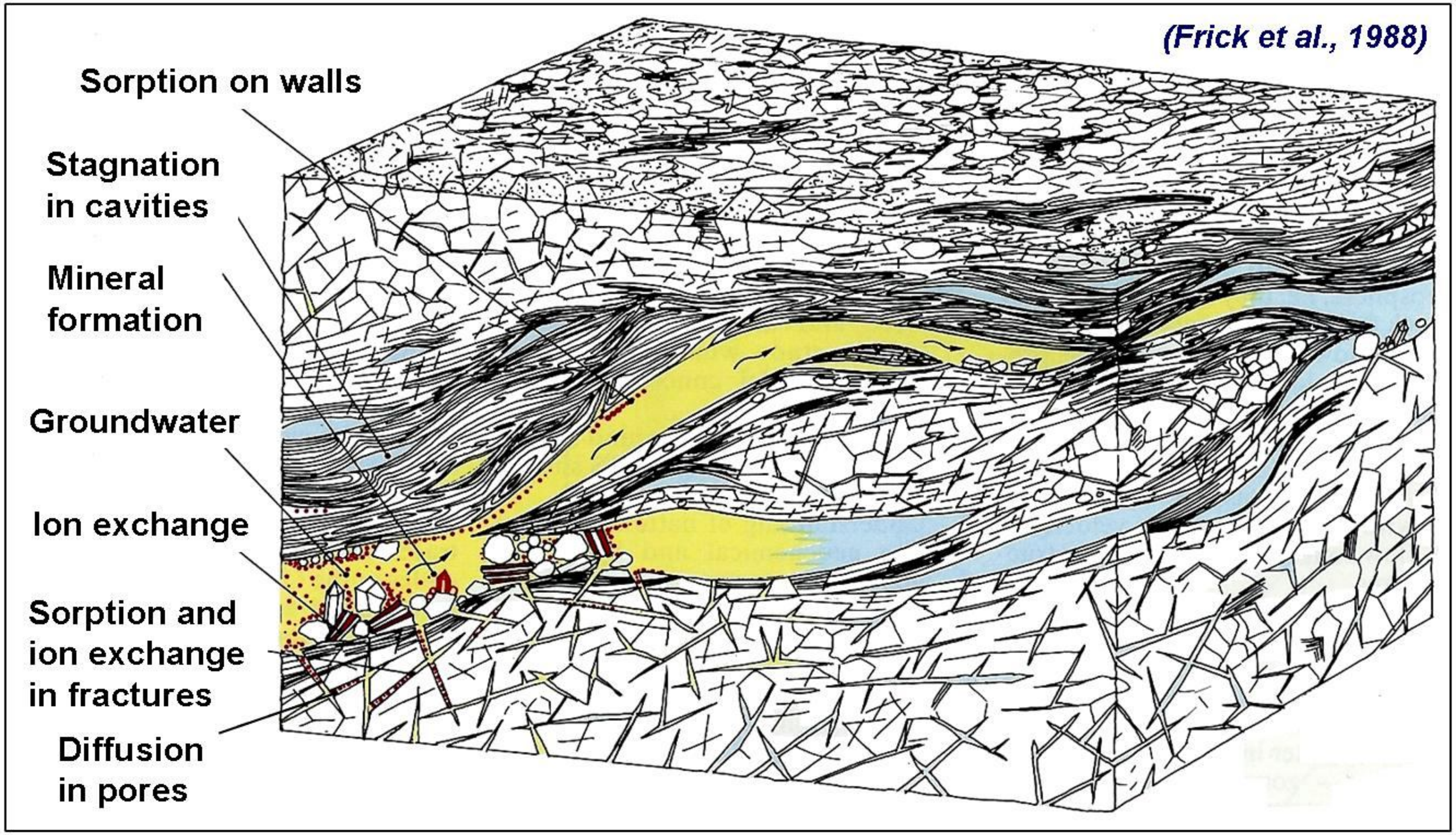

$K_d = C_R / C_W$ (Alexander, McKinley, 1994)

$R_f = V_W / V_C = 1 + K_d \rho / \Phi$ (Freeze, Cherry, 1979)

Density and porosity are the fundamental variables in rocks

Images of geometry and linkage of water-conducting discontinuities

Models

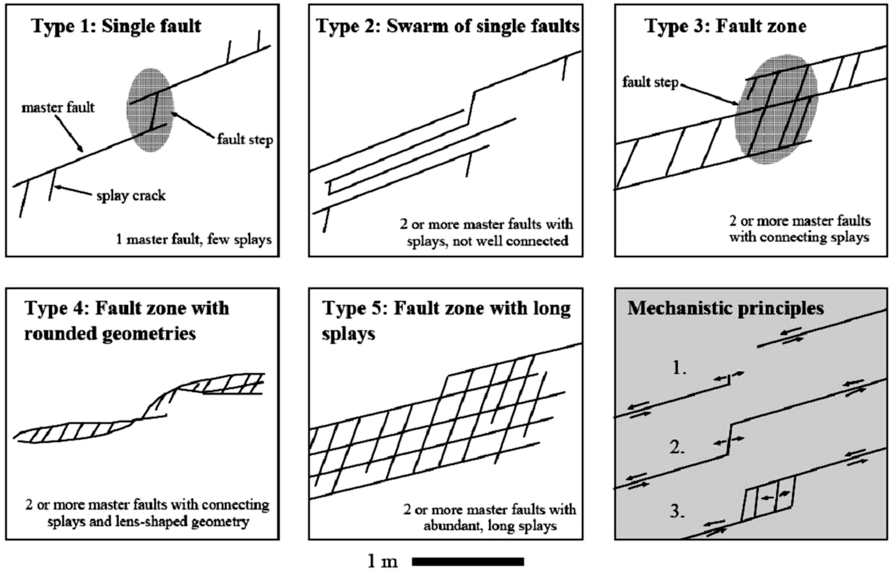

Fault geometries of five types of water-conducting features on a scale of meters *(after Mazurek, Jakob, 2001)*. The sketch in the lower right corner schematically illustrates the evolution of the growth and linkage of master faults and splay cracks, resulting fault steps and locally different fault geometries.

Reality

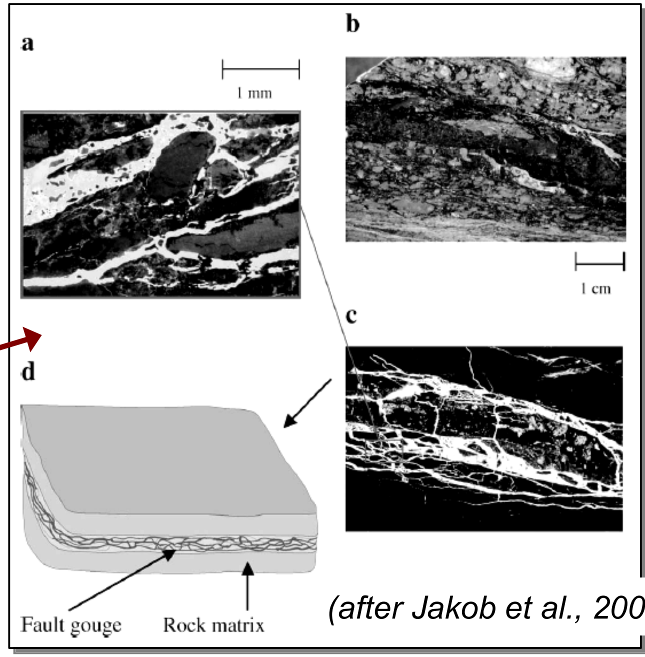

(after Jakob et al., 2003)

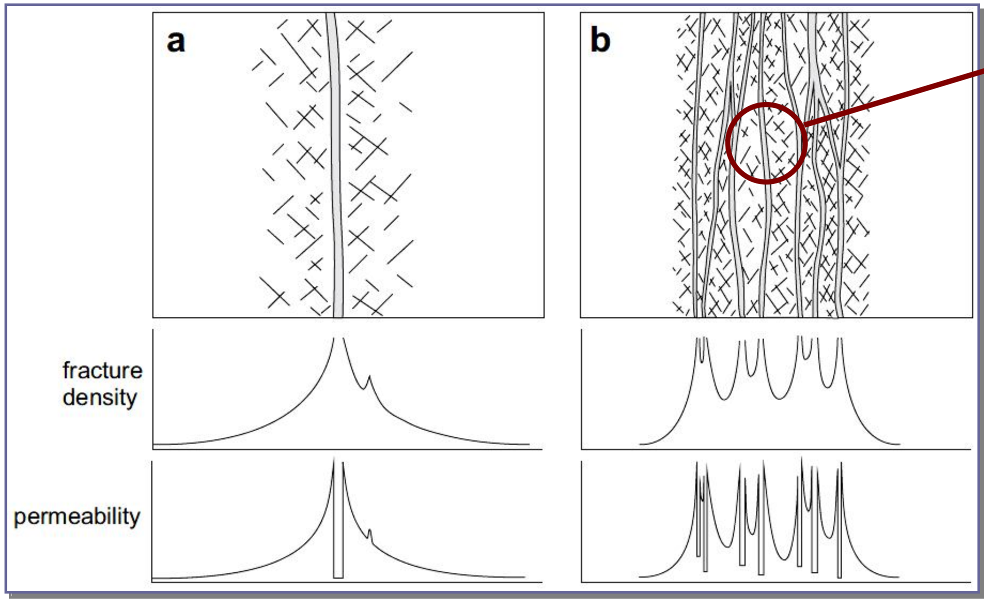

Some physical properties of fault zones related to their structure (damage zone and fault core): (a) single fault core and (b) multiple fault core, which illustrate the resulting complexity in characterizing the resultant filtration-transport properties (*after Faulkner et al., 2010*)

Change of structure of pore-fracture space and effective porosity as a function of distance from fluid-conducting discontinuity

Lab tests

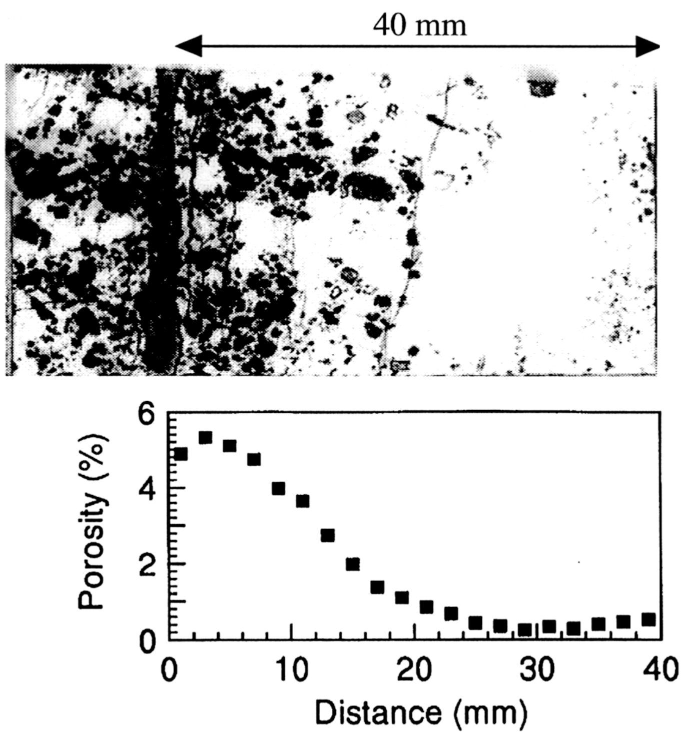

Variation of effective porosity as a function of distance due to 14C-PMMA method (*after Hellmuth et al., 1992*)

Field reality

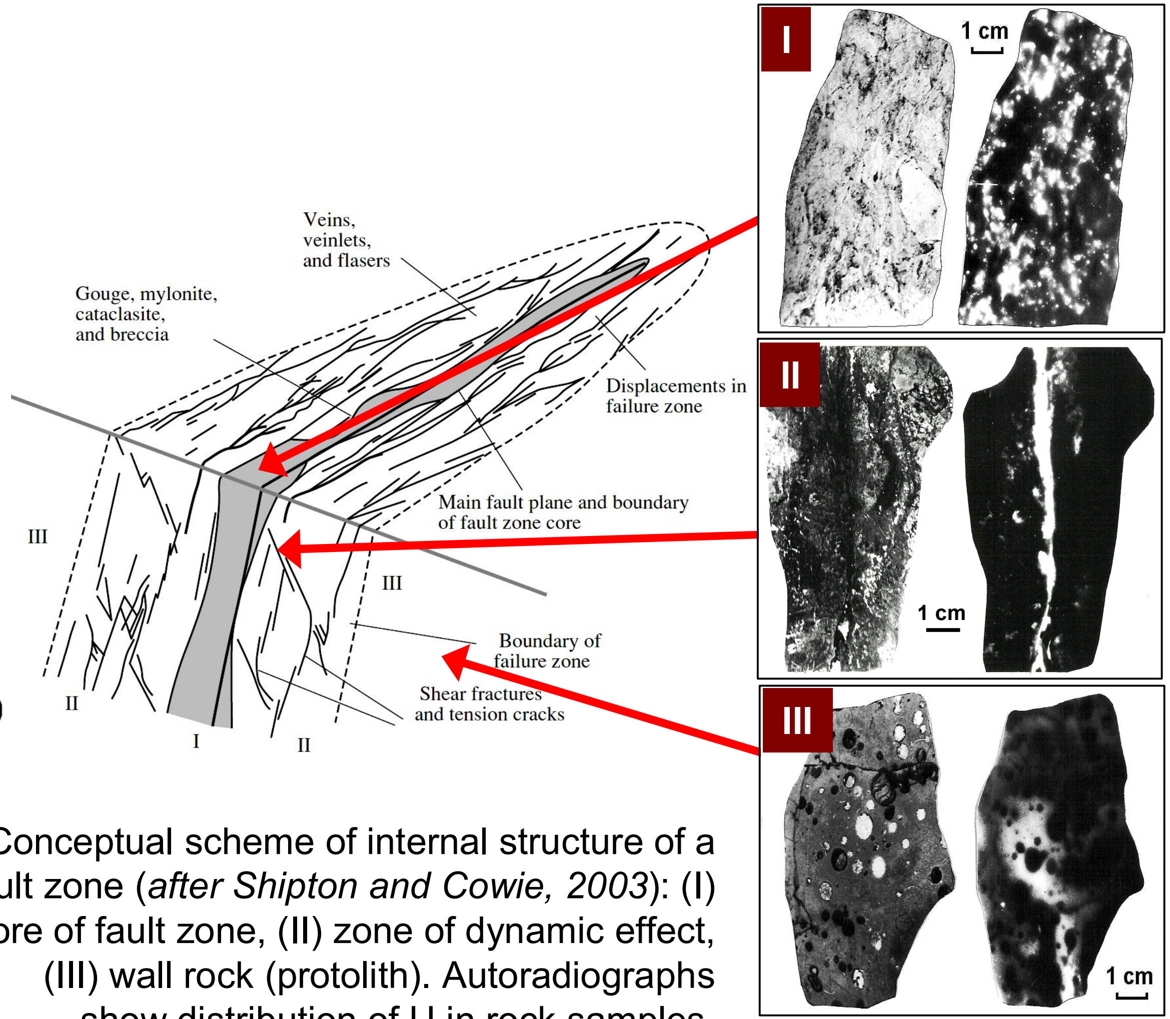

Conceptual scheme of internal structure of a fault zone (*after Shipton and Cowie, 2003*): (I) core of fault zone, (II) zone of dynamic effect, (III) wall rock (protolith). Autoradiographs show distribution of U in rock samples.

Fractionation of actinides (uranium)

Model

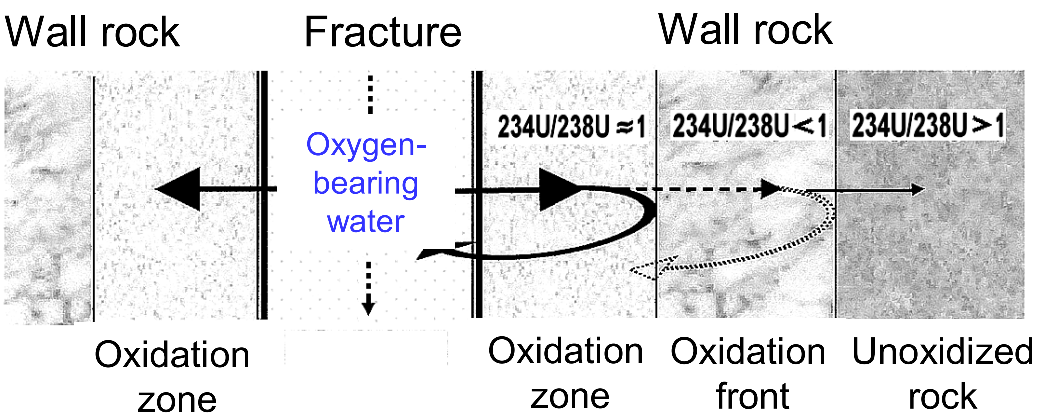

Model of fractionation of uranium isotopes into the fracture – near fracture space (*after Suksi et al., 2001*): application of uranium-series disequilibrium data to interpretation of oxygen intrusion in rocks.

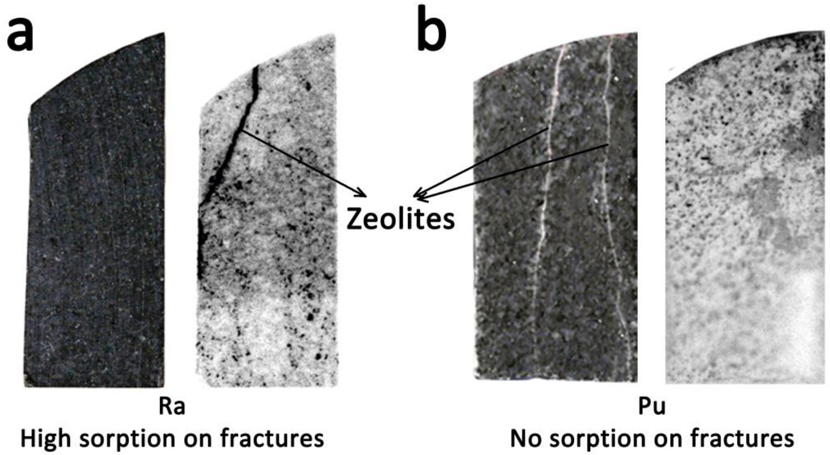

Comparison of optical image and digital radiograms showing radium (a) and plutonium (b) sorption on rock samples of the Niznekansky granitic massif (gabbro-diabase and garnet-biotite plagiogneiss, respectively) (*after Petrov et al., 2018*).

Field / Lab observations

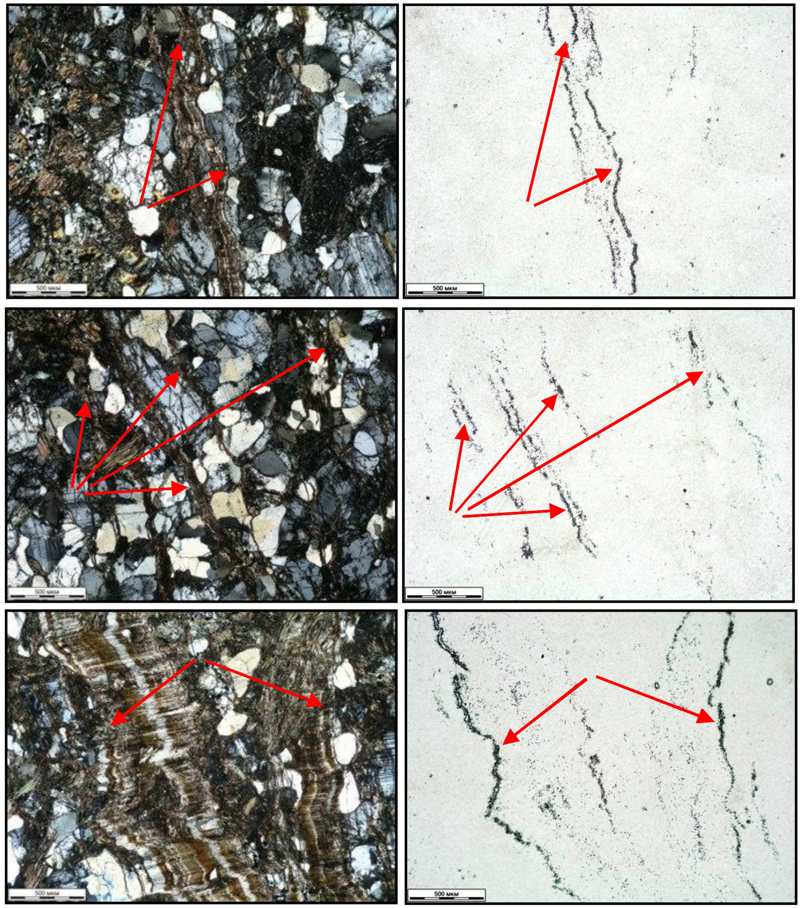

Uranium concentrations (FTR data) along mineralized (Fe-hydroxides) fractures within upper part of the oxidation zone (Niznekansky granitic massif)

Relationship between THMC processes (a) and alternative approaches of imaging geometry and linkage of water-conducting discontinuities in space (b) for filtration-transport modeling

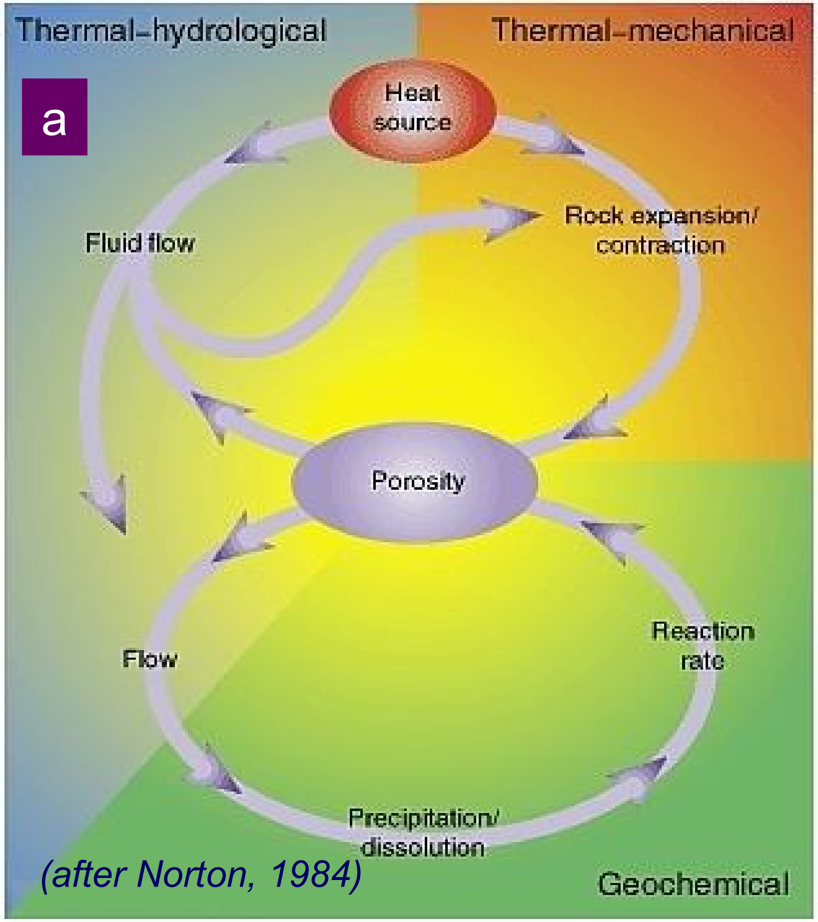

(after Norton, 1984)

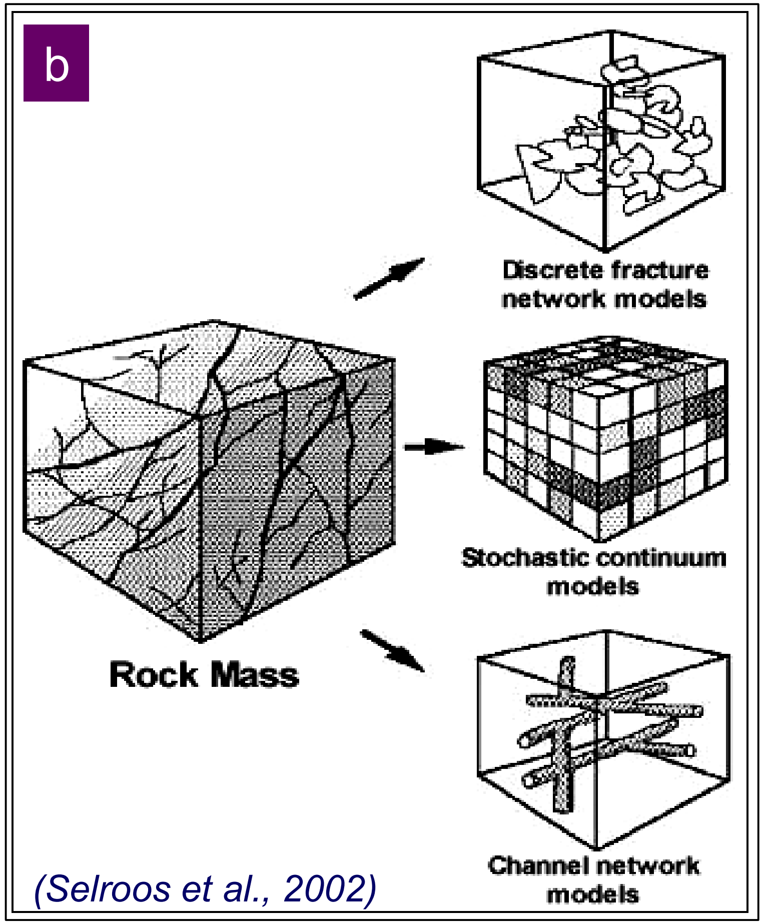

(Selroos et al., 2002)

Realistically simulating a nuclear repository requires the ability to couple the continuous interplay of heat, chemistry, water flow, and rock mechanics. Porosity and permeability are the fundamental variables that link these processes.

Response of fracture pore space on heat and water flow

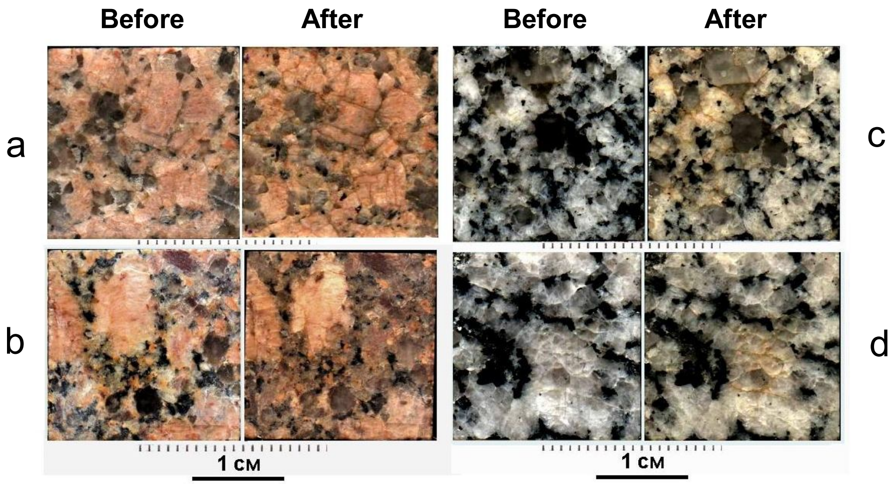

Scanned images of leucogranite (a), porphyritic adamellite (b), porphyritic granodiorite-tonalite (c), and quartz diorite (d) before and after heating up to 250 grad C, which results to transformation of fracture-pore structure.

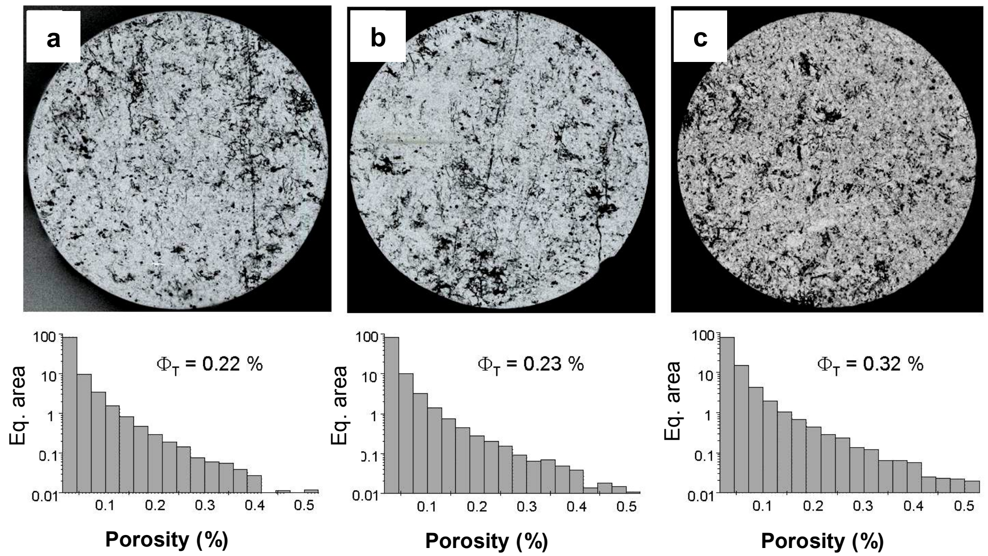

Sequence of opening of pore channels and increase of total porosity (Φ_T) in granitic gneiss during heating from 22 (a) to 60 (b) and 150 (c) grad C. 14C-PMMA method. Time of impregnation by MMA varies from 8 to 12 days.

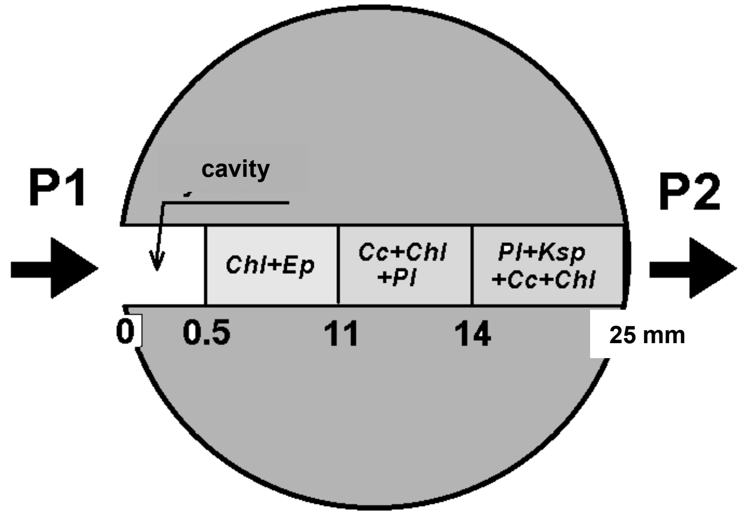

Test on water filtration through artificial fracture in porphyrite (*after Zaraisky, 1994*). Conditions: T = 250°C, P1(inlet) = 146 bar, P2(outlet) = 145 bar, 38 days, water volume = 103.4 cm^3, permeability (mD) 1.0 10^{-1} (initial) and 2.5 10^{-3} (final). Chl – chlorite, Ep - epidote, Cc - calcite, Pl - plagioclase, Ksp – potassium feldspar

Location and traits of the Transbaikal Region

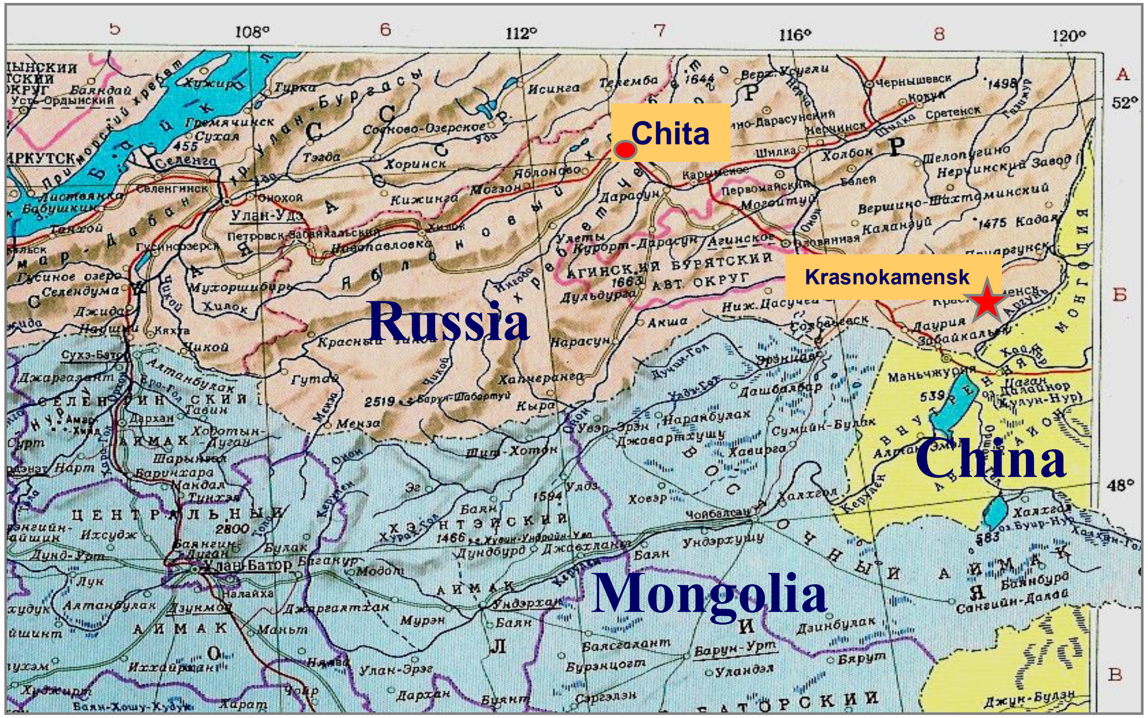

Satellite view of the area with the main faults and caldera edge

- Volcanic Caldera of 20 km in diameter (180 km2) comprises 19 ore bodies
- Host rocks: up to 1.4 km of volcano-sedimentary accumulation within the caldera lying on a granitic Proterozoic basement
- Host structures: Vertical and sub horizontal faults
- Age : Cretaceous (145-140 Ma)
- Ore lies within veins, sub-vertical stockworks and along stratiform layers in the sandstone units.
- Ore: pitchblende, coffinite, and branerite,
- Genetic Model: Hydrothermal remobilisations synchronous of late stage of magmatic activity
- Total initial Resources : 280,000 tU @ 0.2%U
- Production : ~140,000 t U from 1968 to 2013, 2,133t in2013

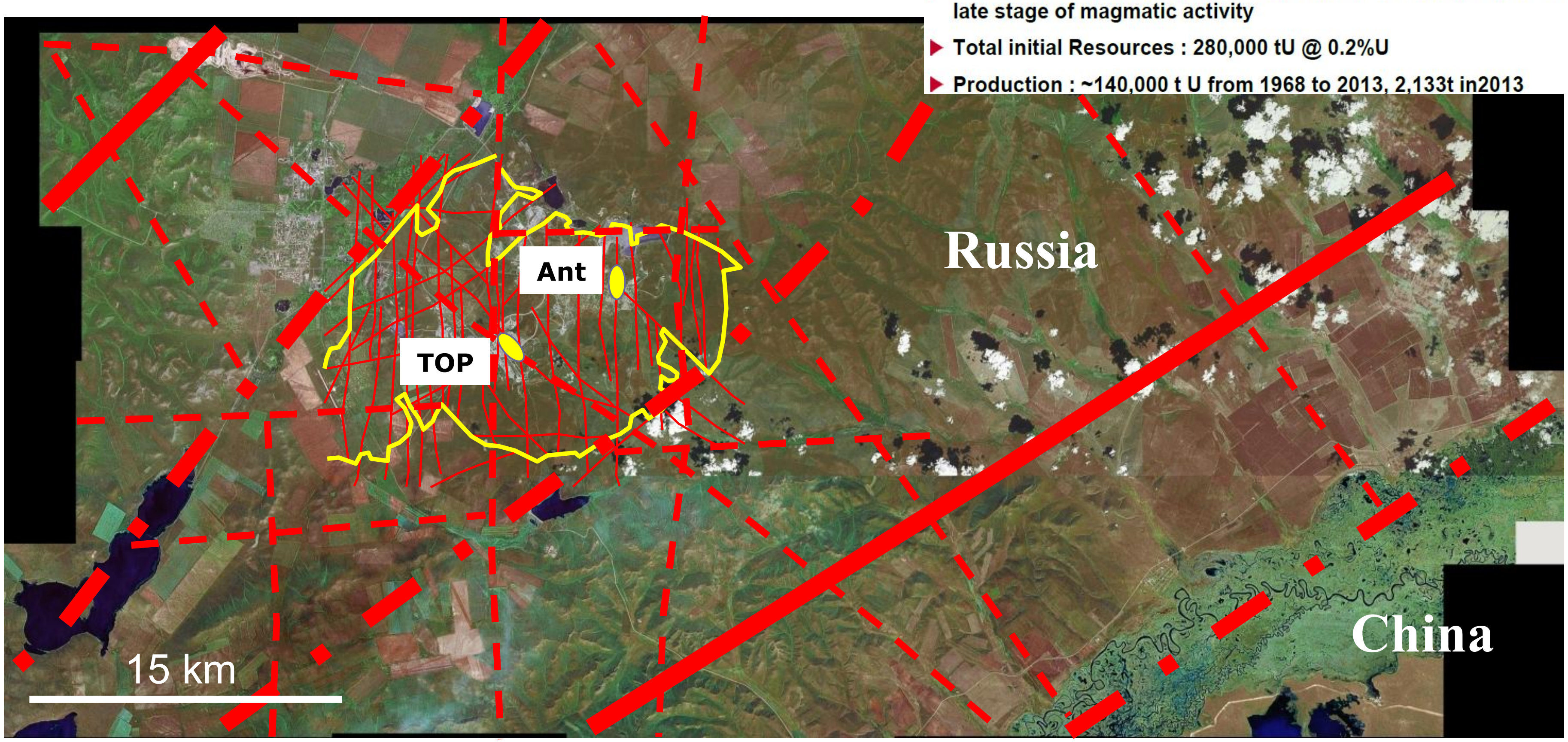

Uranium transfer: environmental and natural resource issues

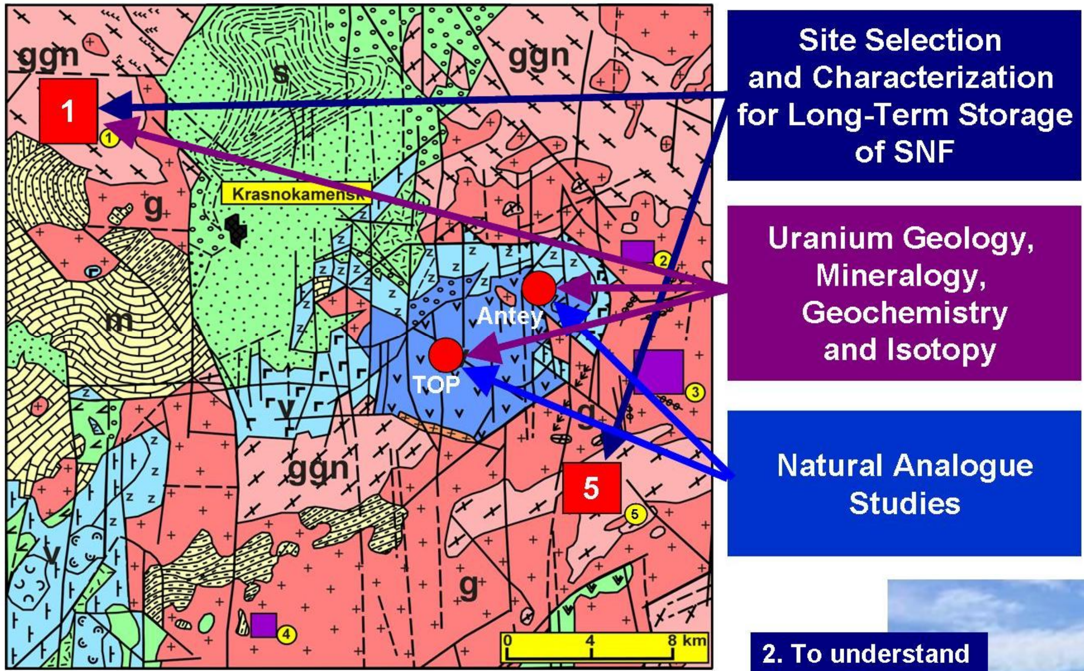

Sites under investigation and main objectives inside and outside of the Streltsovskaya caldera

One of the main objectives is to improve data on processes governing U migration and accumulation in oxidizing-reducing conditions of fracture porous environment

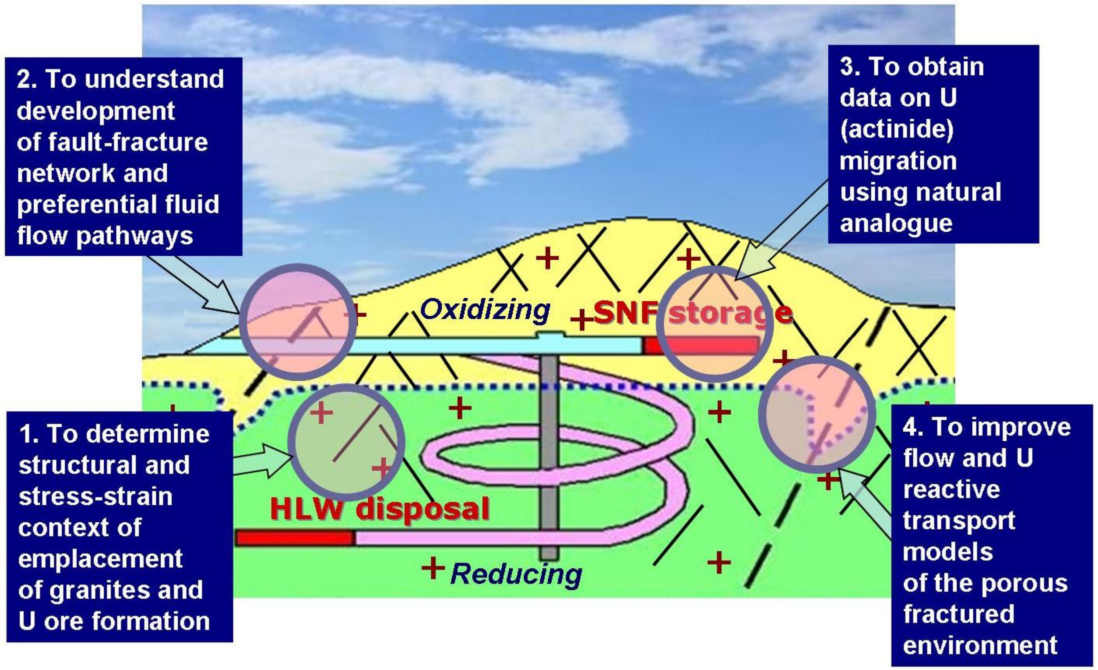

Some issues of natural analogue studies at deep levels of geological formations

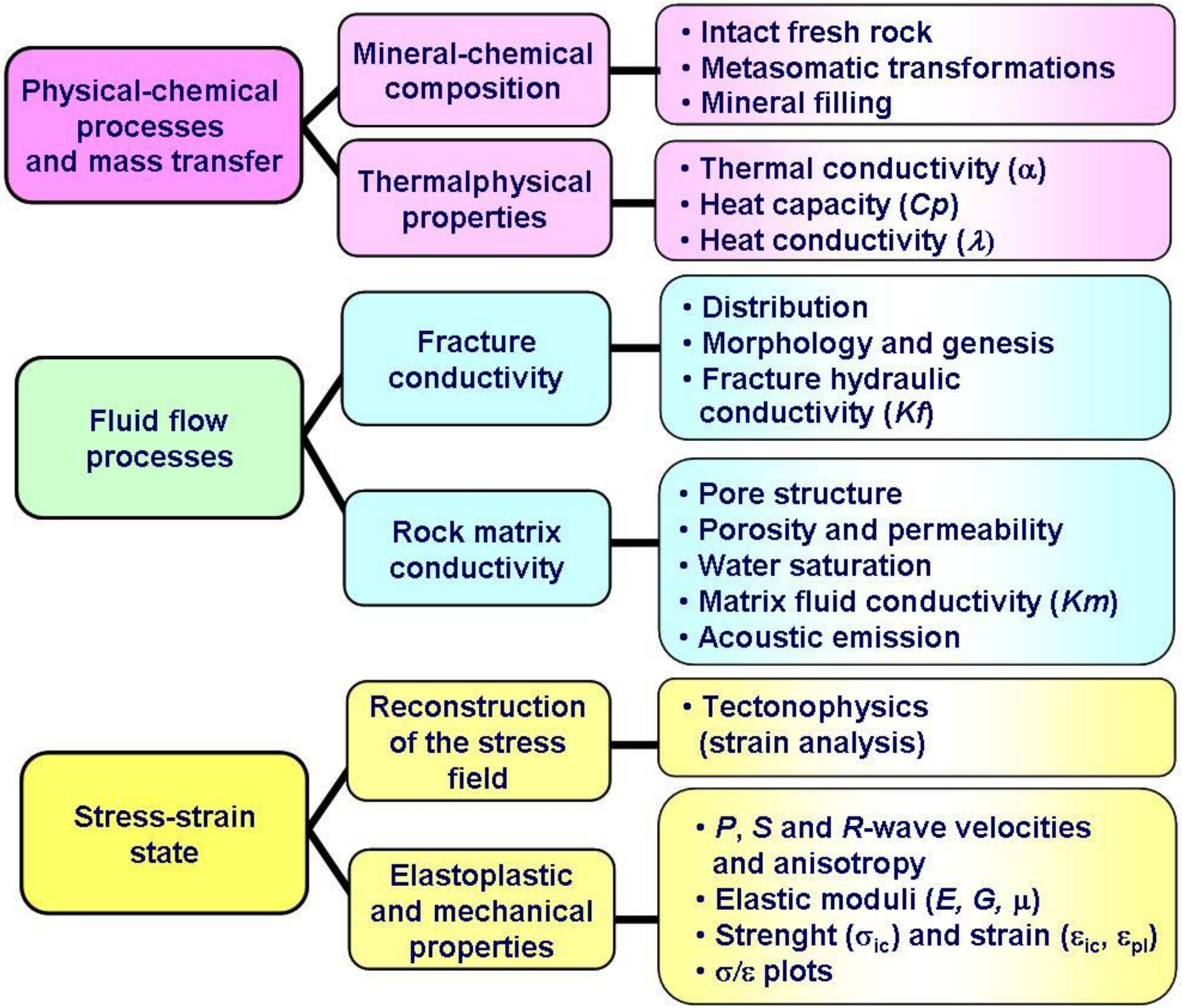

Geologic section of the Antey-Streltsovskoe U deposit (a), photomosaic map of underground opening (b) and autoradiograph of the vein-type mineralization (c)

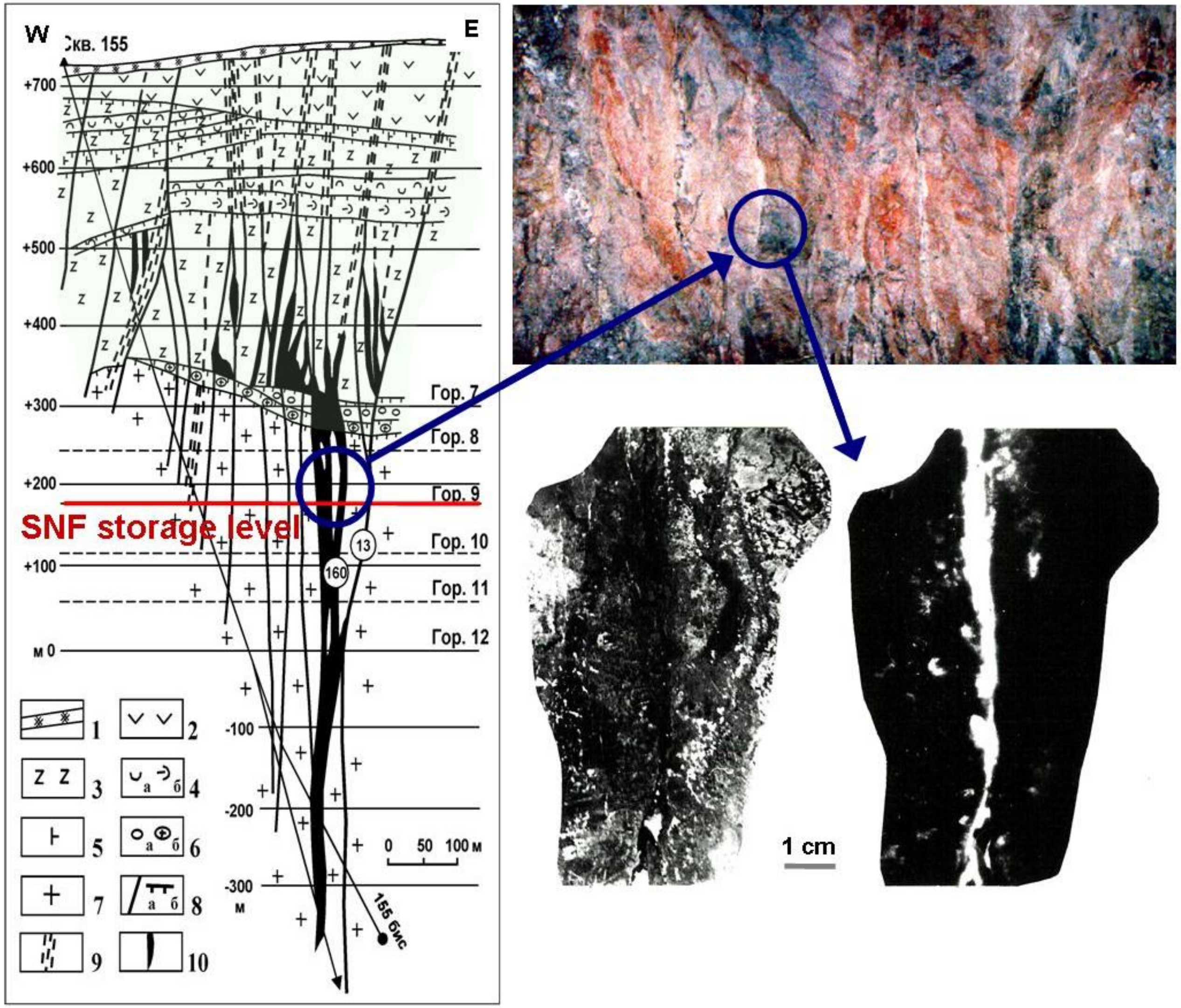

Site specific geological conditions

U mineralogy, geo-chemistry and isotopy

Structural and physico-chemical conditions for U transfer and localization of ores

3D database of the mining area for prospecting and exploration needs

SNF storage facility analogue studies

Natural analogue studies: for needs of SNF storage facility operation

1) orebodies are composed by pitchblende UO2 = SNF analogue

2) orebodies are enveloped by packets of hydrothermally altered rocks (hydromicatized rocks and low-temperature mineral assemblages as analogue of backfill material)

3) packets of altered rocks are localized in fresh granite (the enginering disturbed zone and far-field of an SNF facility)

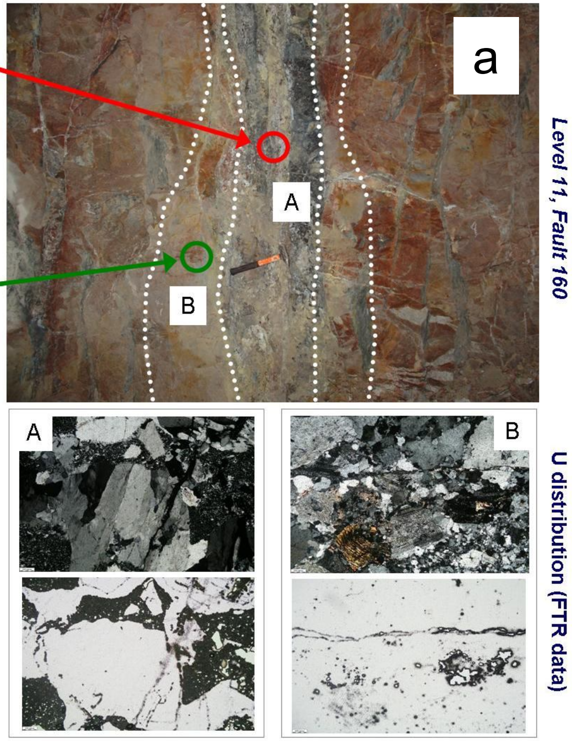

(a) Analogue of constructional elements of SNF storage facility. An example of the Antey U deposit

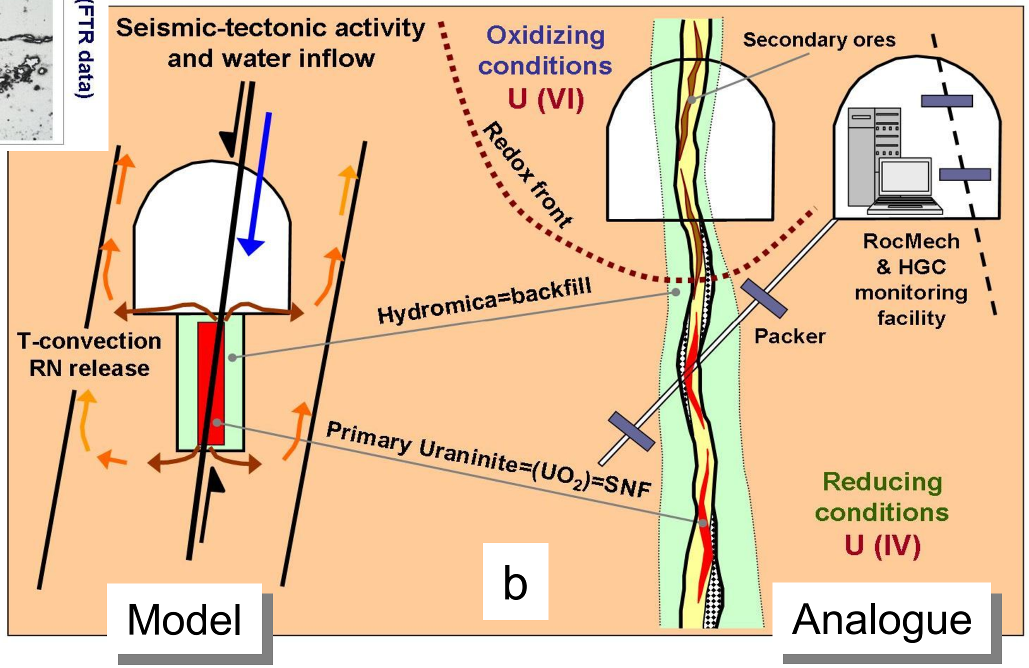

(b) A set of tools for detailed examination of probabilistic scenario of the thermohydromechanical and chemical (THMC) processes including rock burst (c)

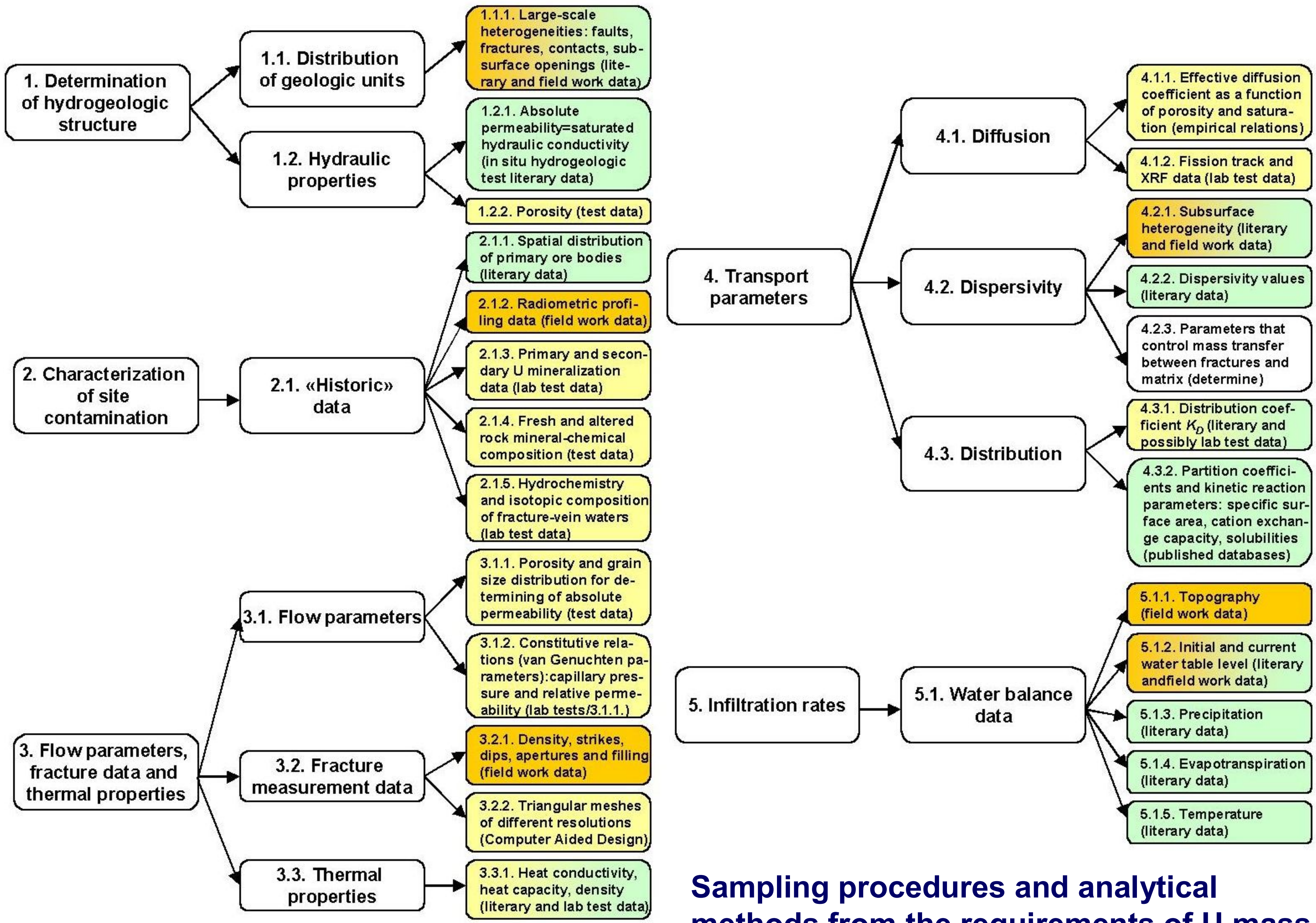

Sampling procedures and analytical methods from the requirements of U mass transfer modeling for vadose zone

The Tulukuevsky Open Pit (TOP): 50,000 tU@0.2%U

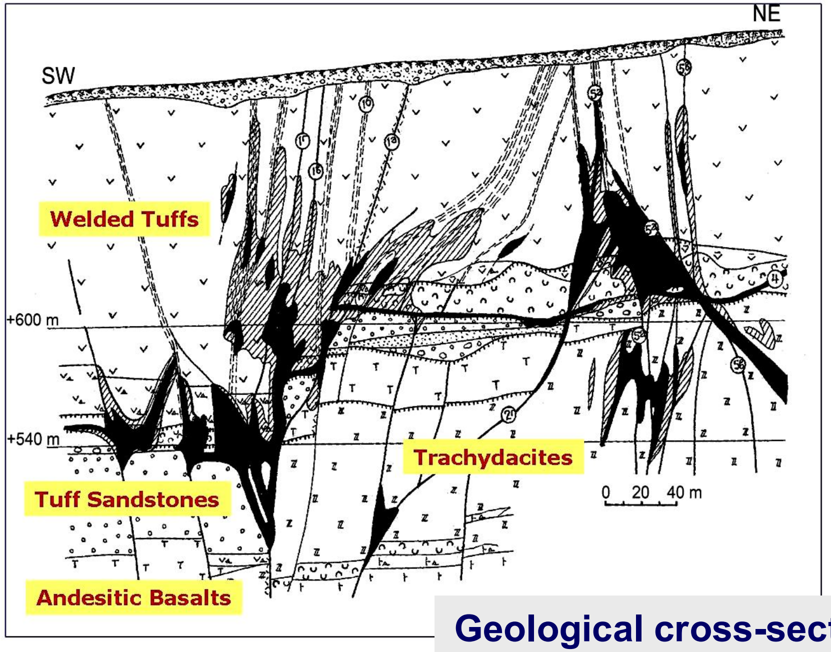

Geological cross-section

Surveying plan

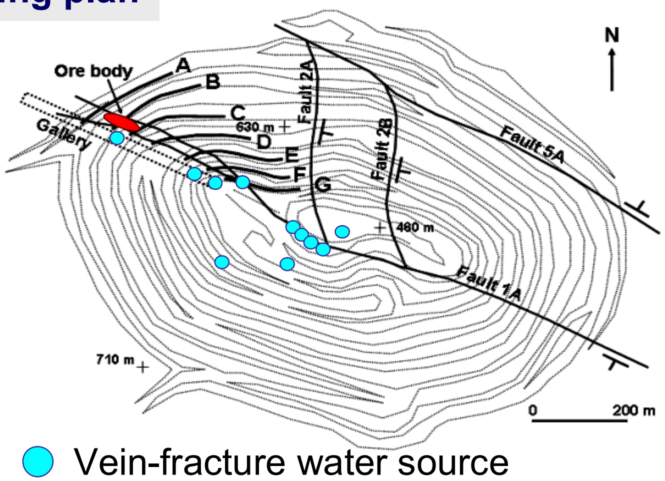

Dynamics of water table recession and changing of oxidizing/reducing conditions during the TOP mining

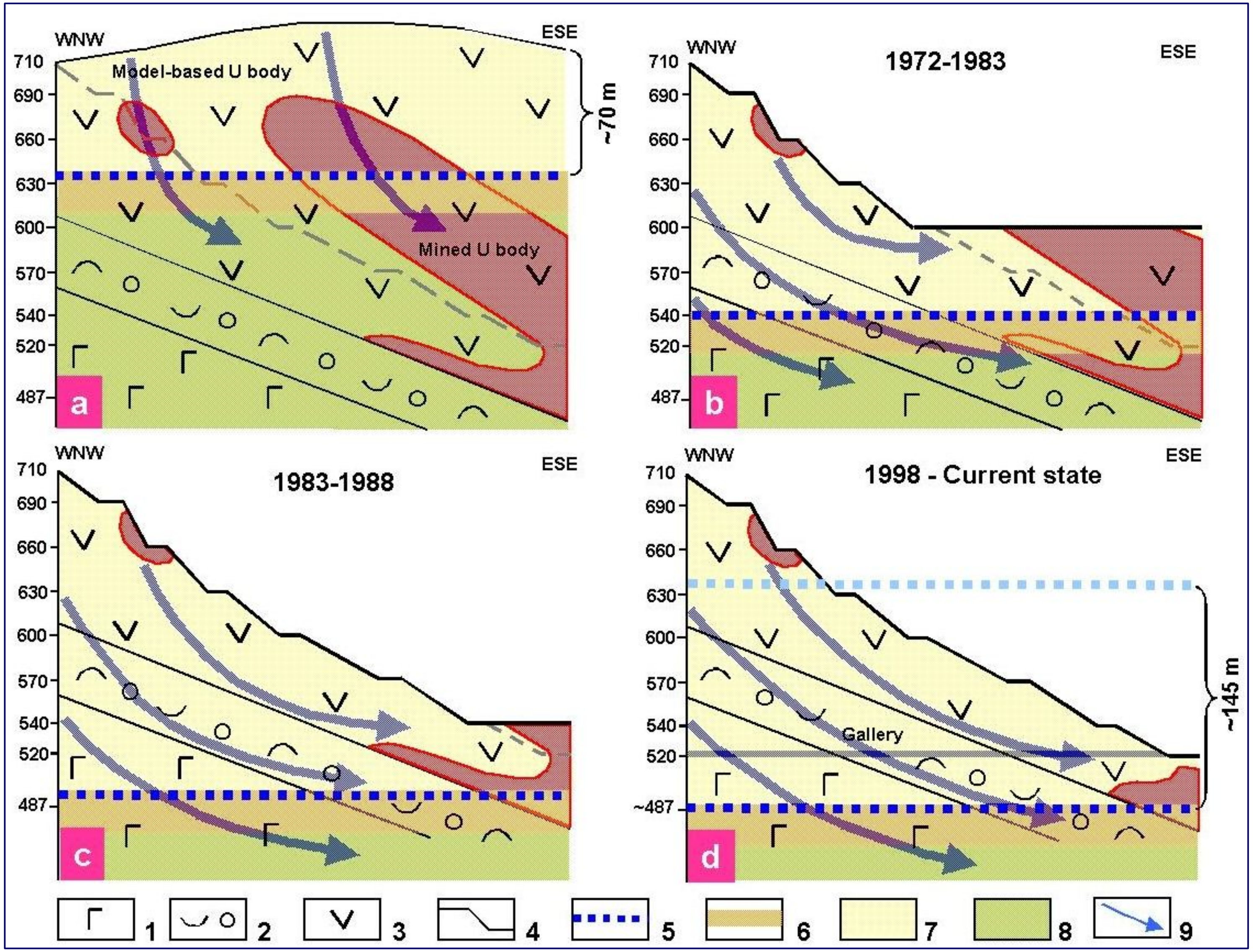

General view of the NW block with mineral zoning of hydrothermal and hypergene transformations of rocks

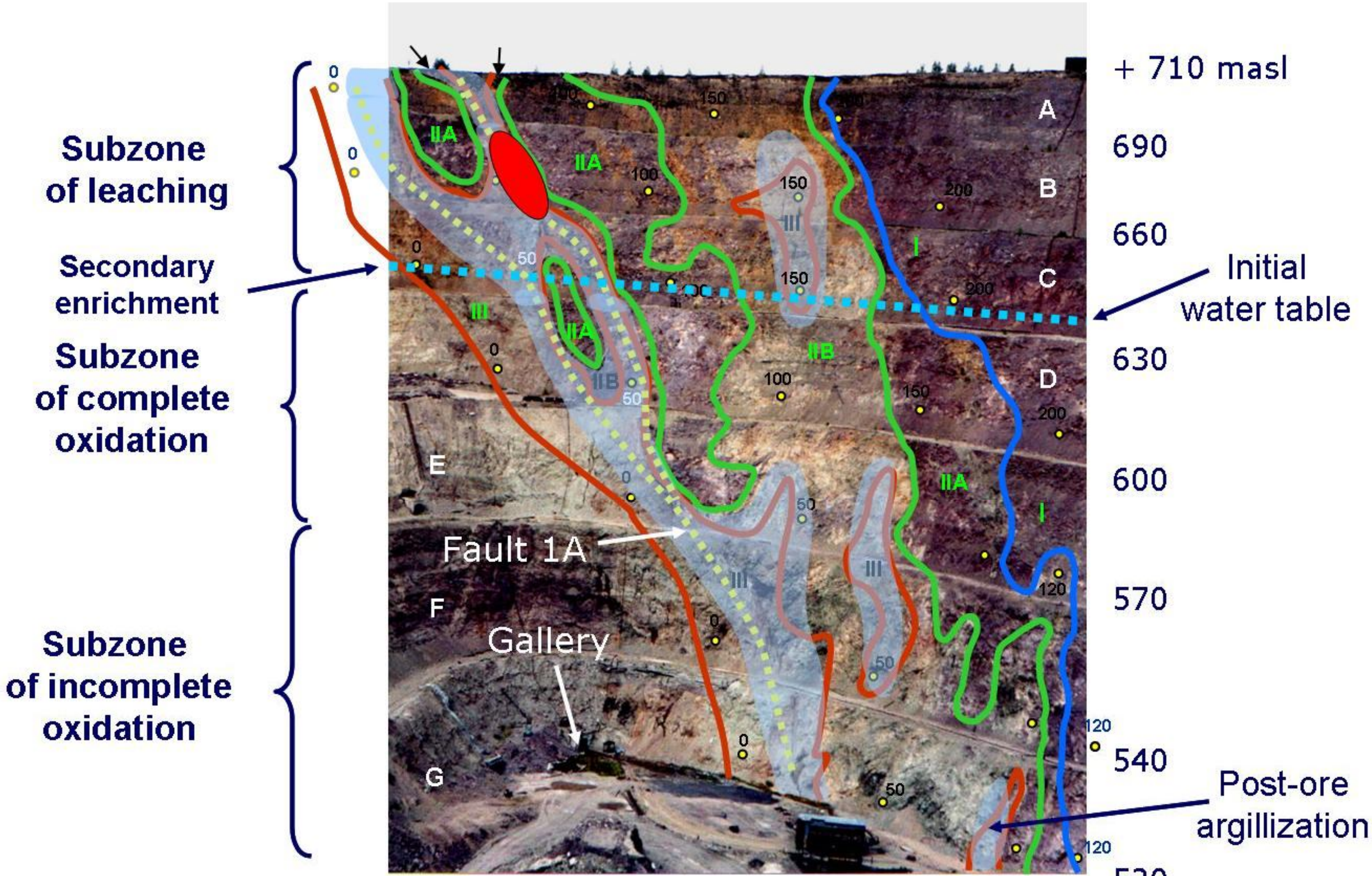

I - external (relic: KFs, Olg, Q, Bt, Hem / neogenic: Ilt-Sm, Car)
II - intermediate (Q, KFs, Alb / Ilt-Sm, Car, Q, LA)
III - internal (Q, KFs / Q, Ilt-Sm, Car, Hem, LA, Ber, Kaol)

Pitchblende (a) and pitchblende-molibdenite (b) ores and consecution of U mineralization

Time consecution of U mineralization:

Hypogene (pitchblende and tucholite)

U minerals of the ancient oxidation zone (beginning: blacks and urhyte, completion: uranophane)

Secondary (uranophane, heyviite, calcurmolite, liebigite etc.)

TEM images and EDS of uranophane development from metacolloid (a) and protocrystals (b, c) to crystals (d)

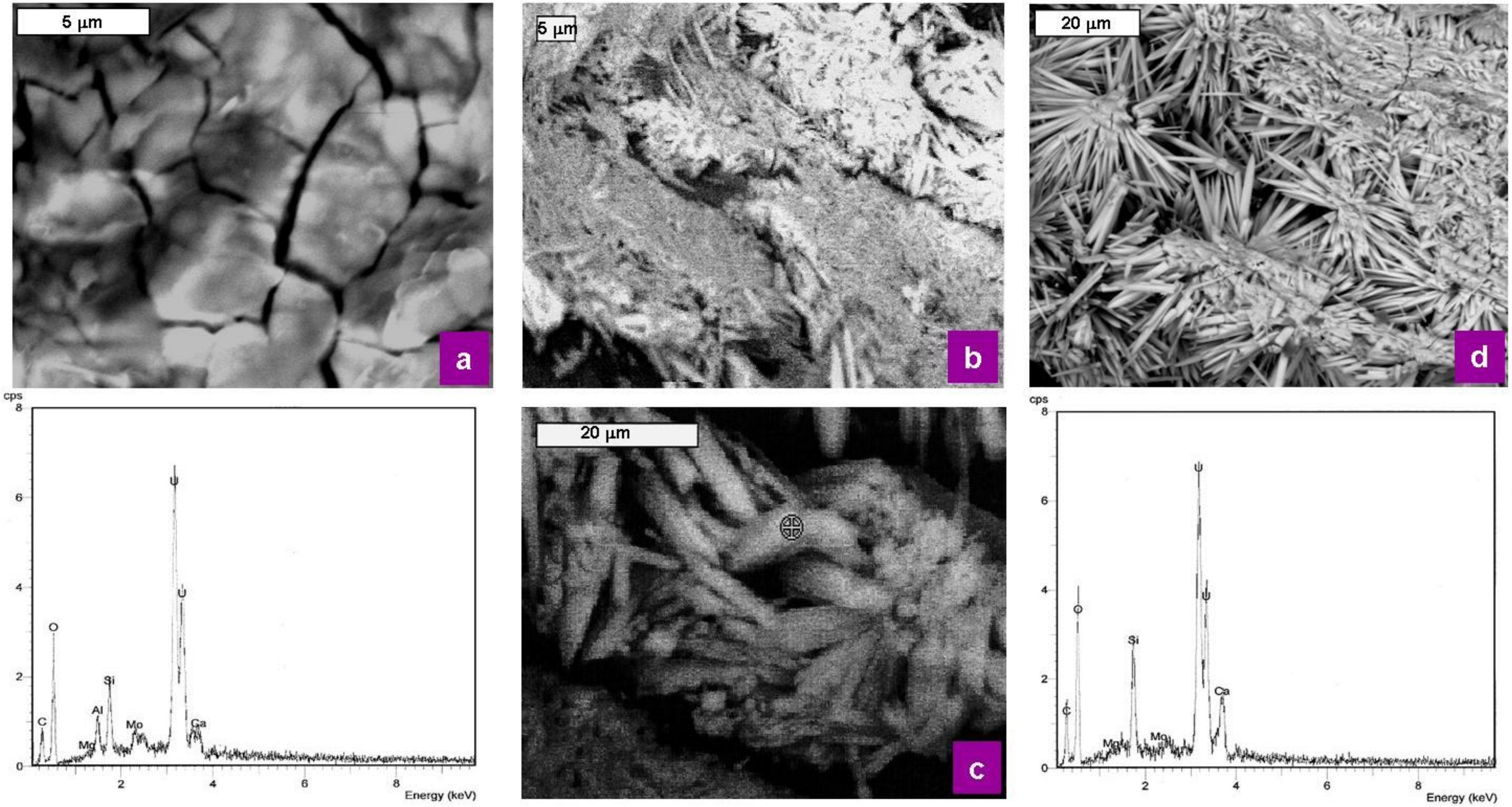

$U^{IV}O_2 + O_2 + H_2O \rightarrow U^{VI}O_3nH_2O + Me \rightarrow MeU^{VI}{}_2O_7nH_2O + Si \rightarrow Me(UO_2)_2[SiO_4]_2nH_2O$

Pitchblende → **Blacks (H-pitchblende)** → **Hydroxides (velsendorphite)** → **Silicates (uranophane)**

Distribution of U in biotite and U content in welded tuffs according to Fission-Track Radiography data

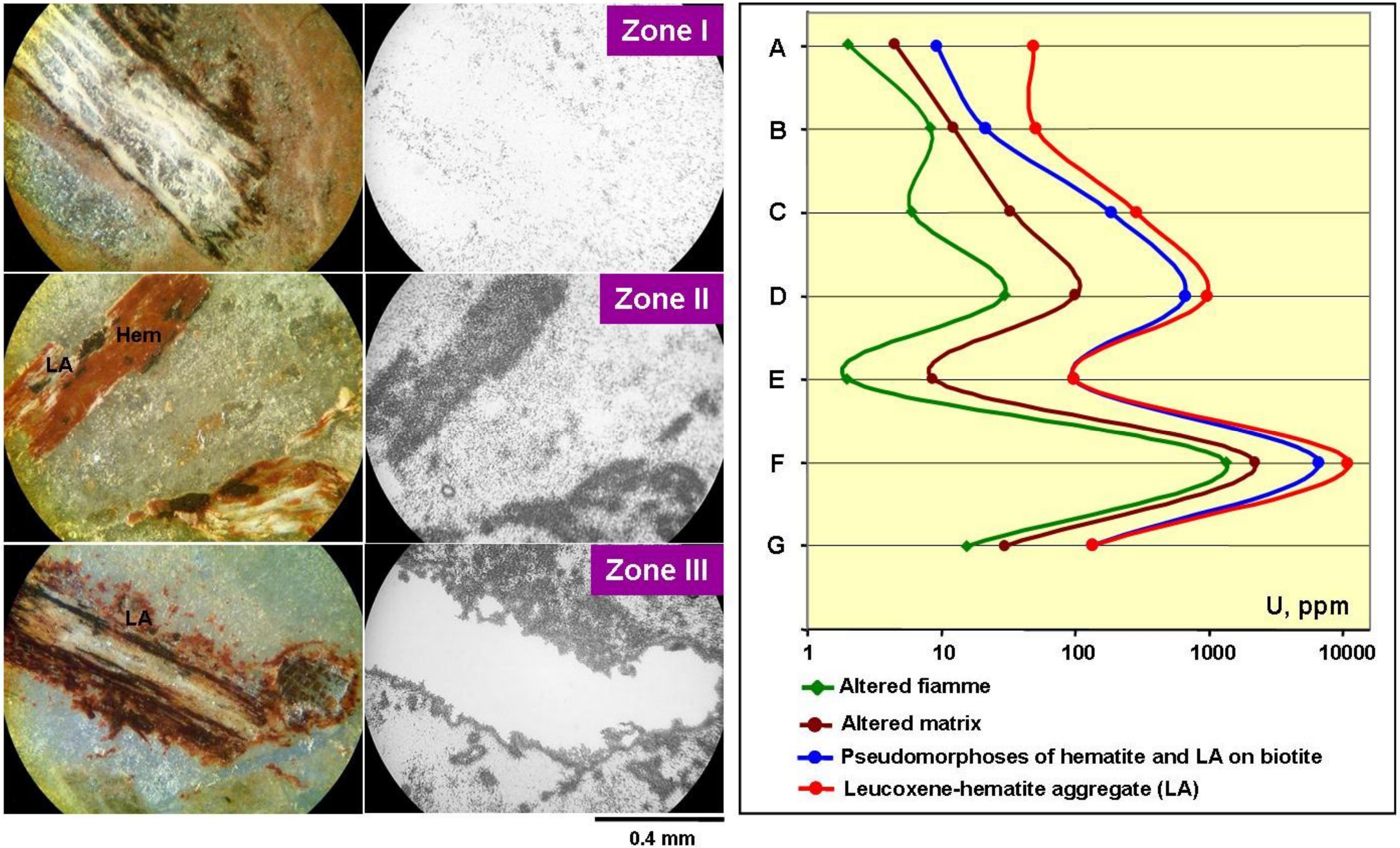

Detection of filtration properties of fluid-conducting discontinuities

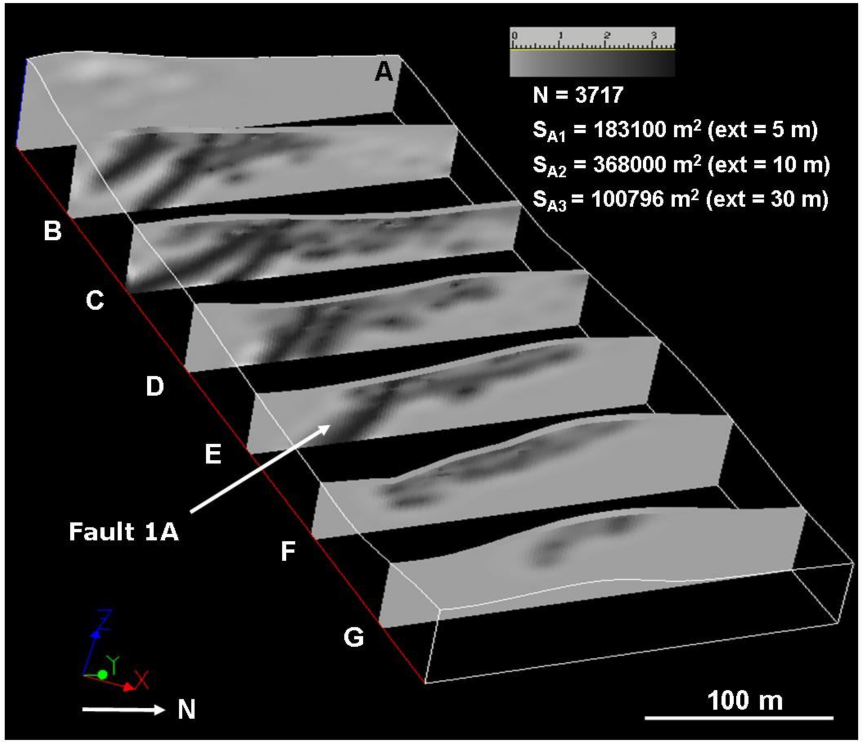

3D GoCAD model of fracture aperture (A), length (ext) and total area (S) at different levels of the TOP. Constructed together with J. Sausse, UHP, Nancy

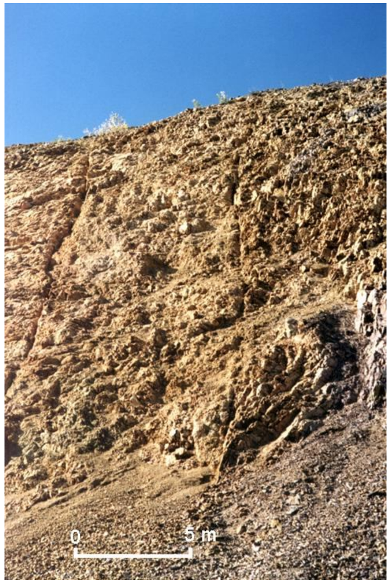

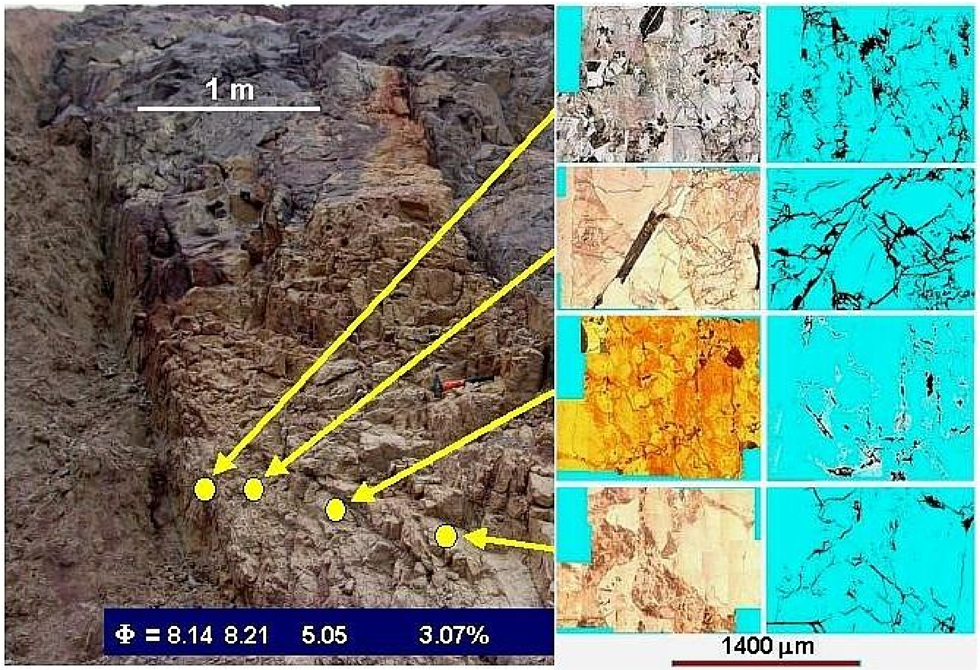

Effective porosity (Φ) and structure of pore space (resin impregnation) as function of distance from hydraulically active fault

Major element distribution pattern in welded tuff

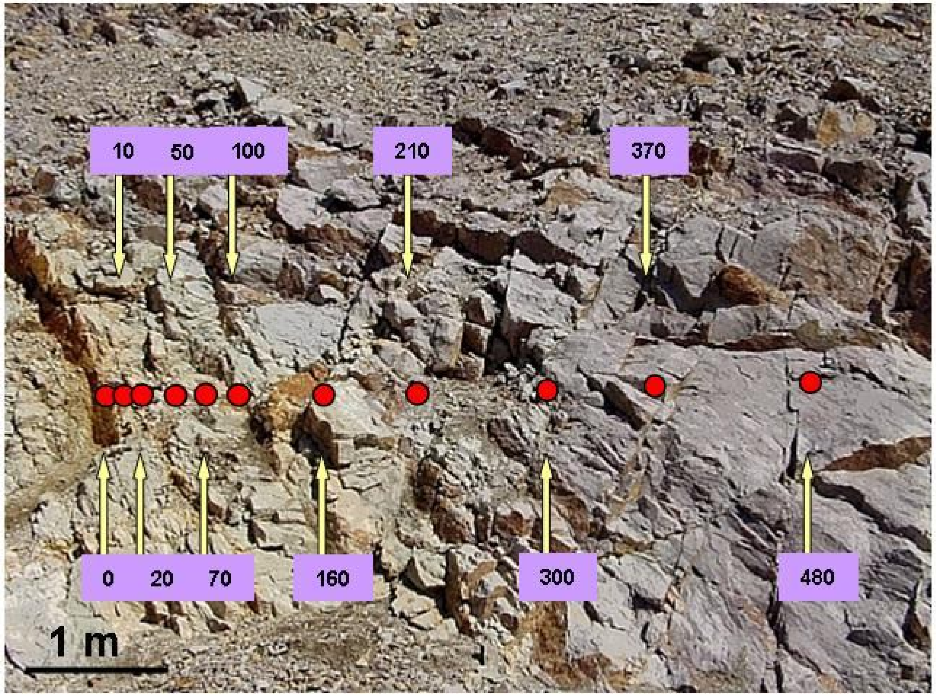

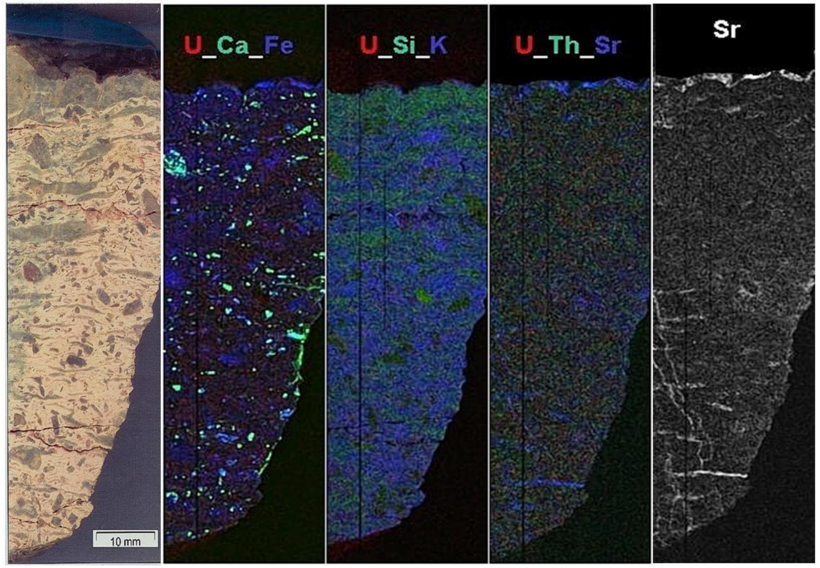

The Sr distribution in welded tuff replaced with hydromica at a distance of 50 cm (sample J3) from the core of hydraulically active fracture is shown leftmost. The elevated Sr contents (white) in carbonate microveinlets and flasers (invisible to the naked eye) are shown rightmost (μ-EDXRF scanning and isotopic geochemistry data)

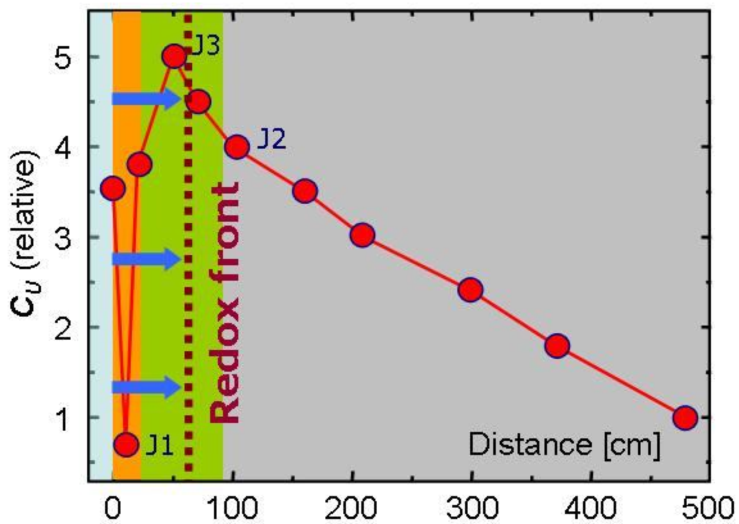

Content of U as function of distance from fluid-conducting fracture (FTR data)

Evolution of the porosity as function of distance from the fluid-conducting fault according to resin impregnation technique

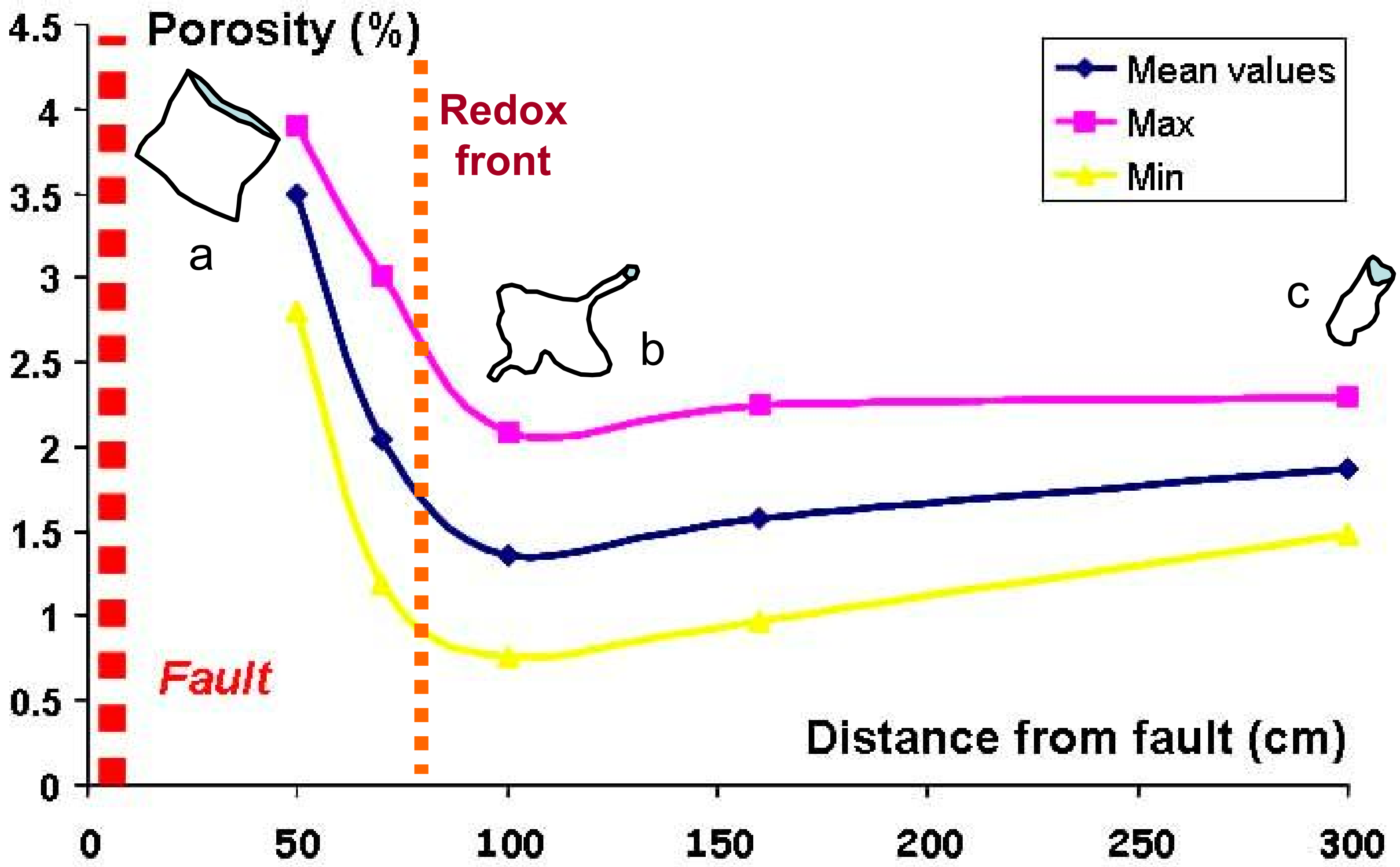

Note the evolution of the micropore shapes from slit-like (a) and bottle-like (b) to cylindrical (c). The shapes are determined by water centrifuge method. Electron microscopy is needed!

Values of $\delta^{18}O$ (a) and U_{total} (b) in rocks as a function of distance from the Fault 1A and single fracture (c)

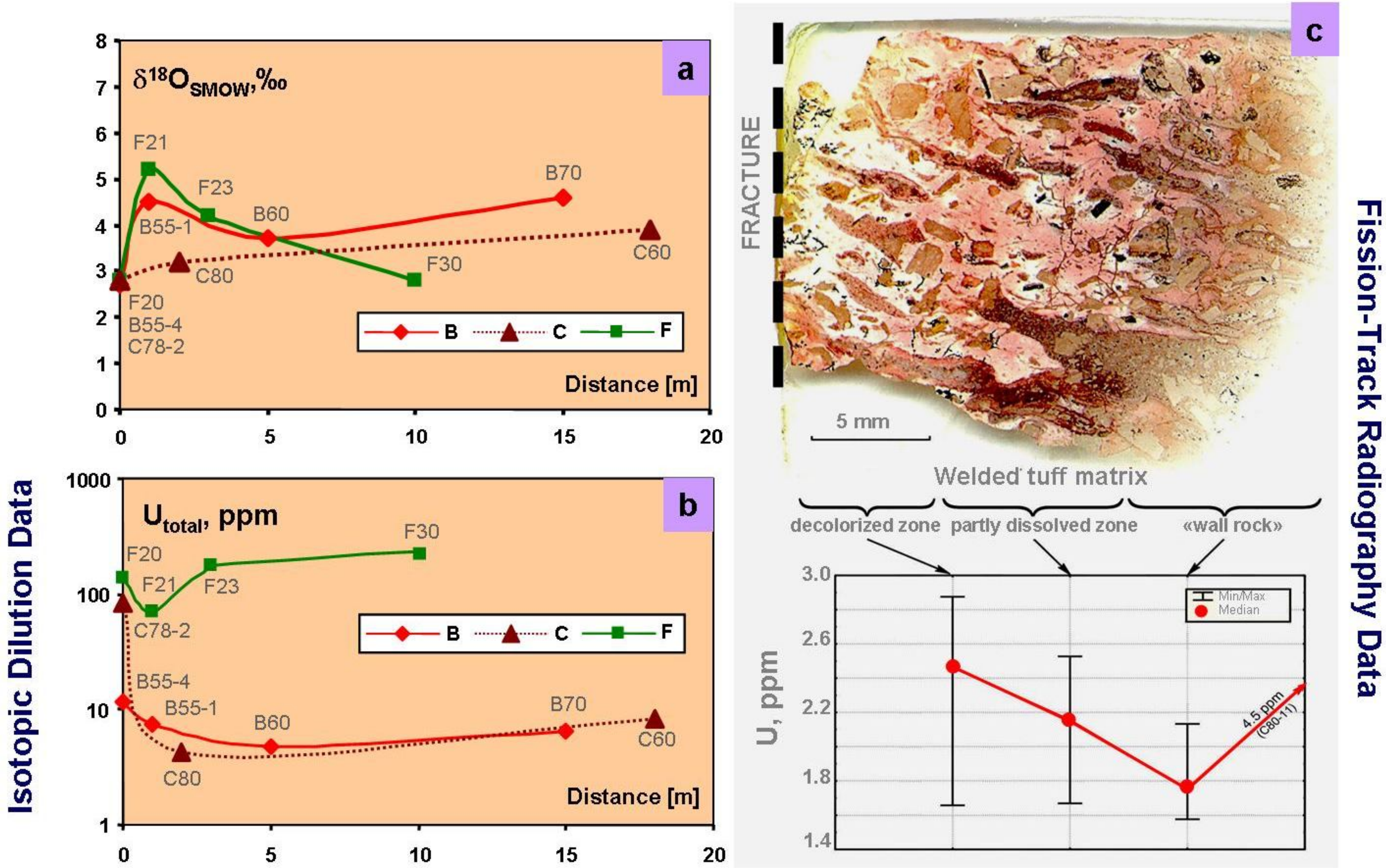

Conceptual model of temporal changes in U content within the profile

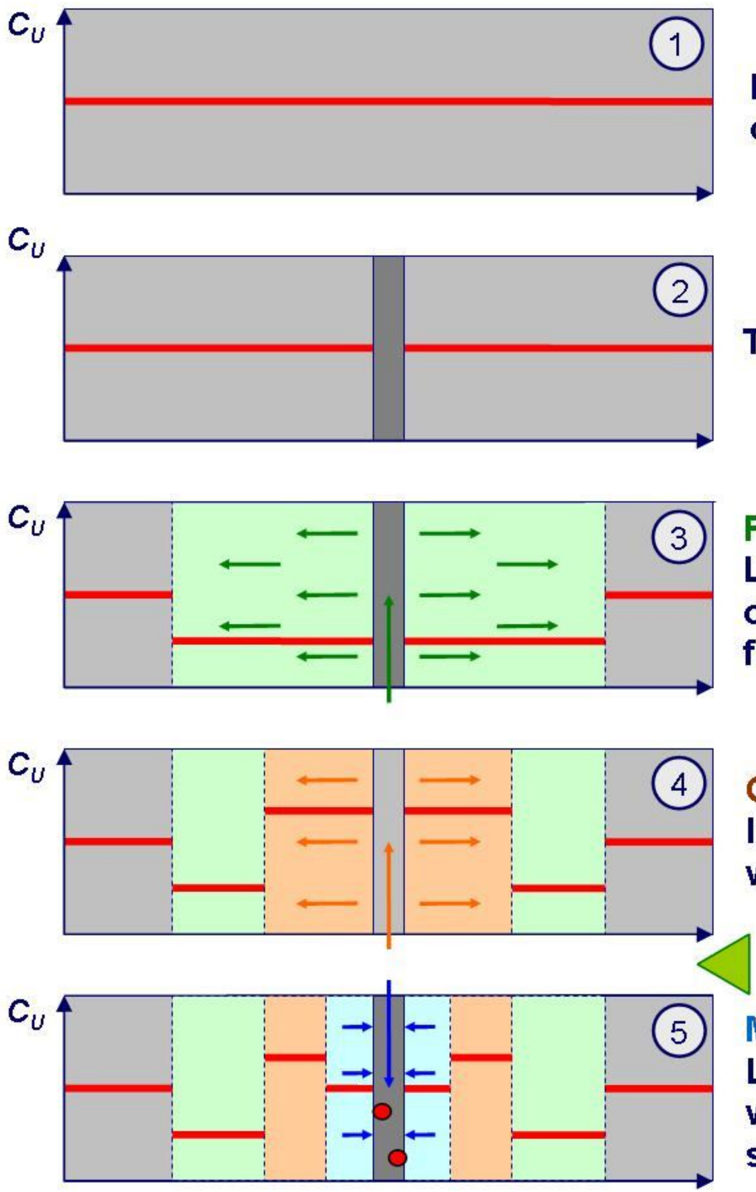

Initial distribution of U in volcanic rocks

Tectonics

Pre-ore hydro-micatization: Leaching and redistribution of initial U within the near-fracture space

Ore-related hematitization: Intake and redistribution of U within the near-fracture space

Post-ore argillization

Meteoric water impact: Leaching and redistribution of U within the near-fracture space, secondary U mineralization

Organic matter content (a) and TEM images of protoferrihydrite (b) and ferrihydrite (c) with goethite and hematite on aggregate flanks

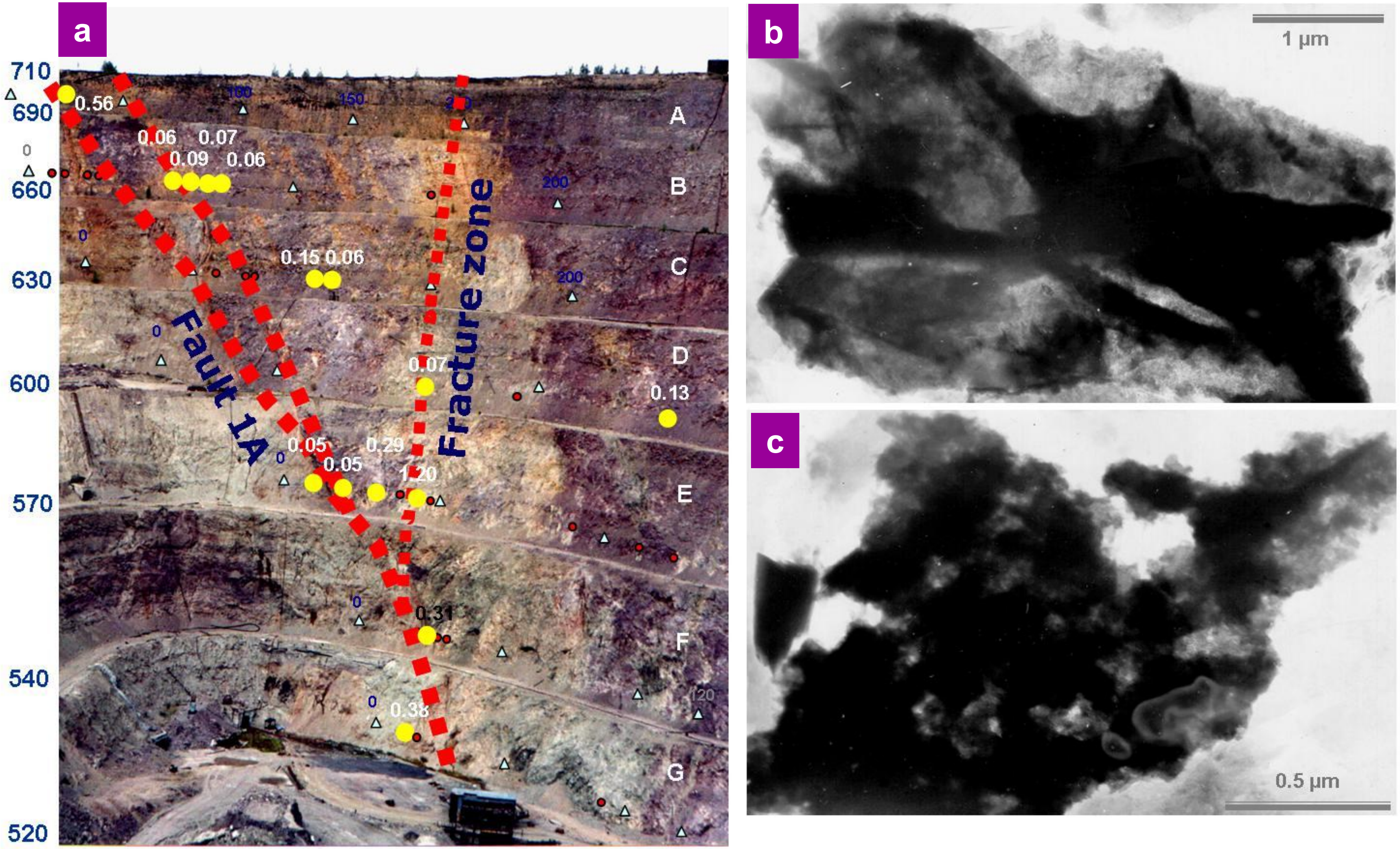

Globular segregations of tucholite (a, b) and secondary uranophane (c) on tucholite

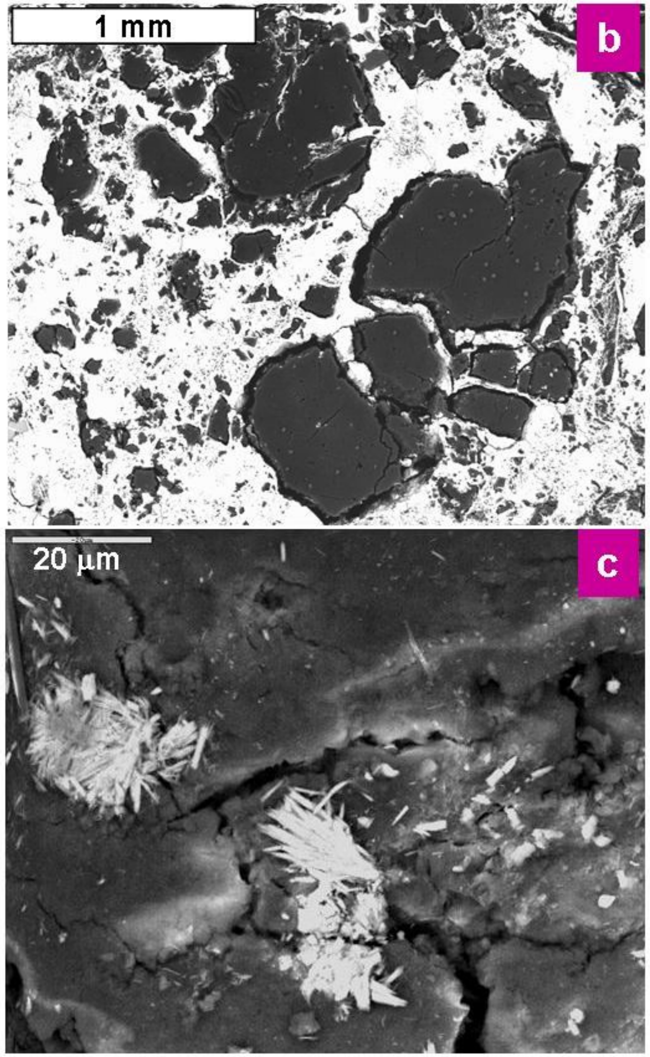

***a** – photography, **b** and **c** - BSE compo images*

Chemical composition of tucholite (mass%): **C 49.47**, O 29.08, Mg 0.28, Ca 1.58, Al 0.81, Si 0.43, S 0.59, **U 10.72**

Hydrochemistry of fracture-vein waters and atmospheric precipitates of the TOP (2002-2015)

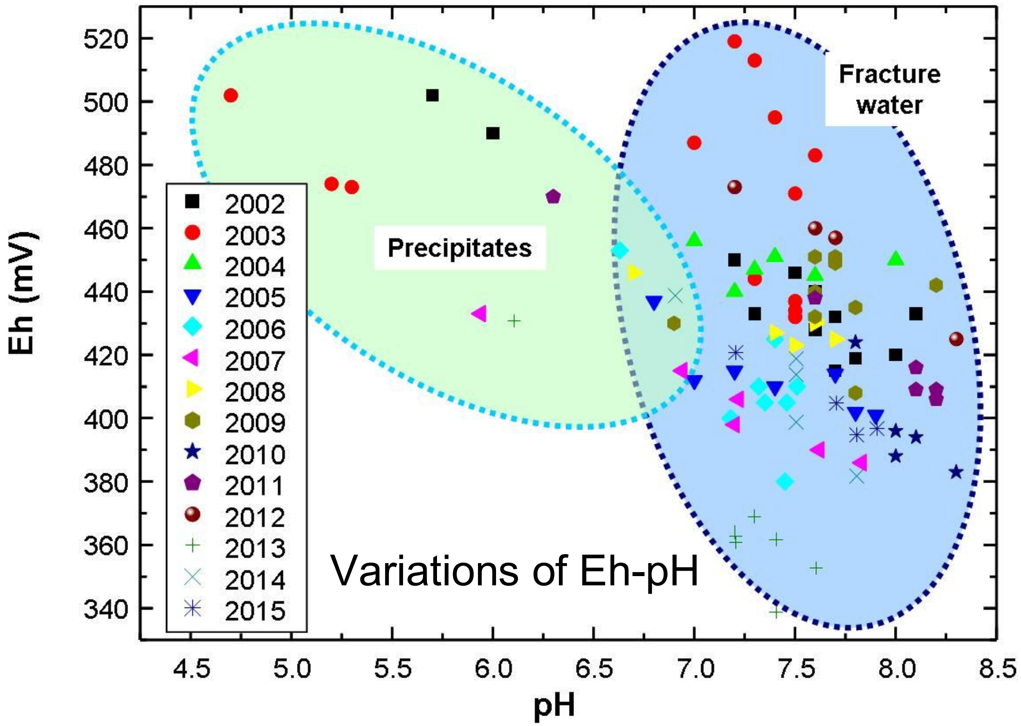

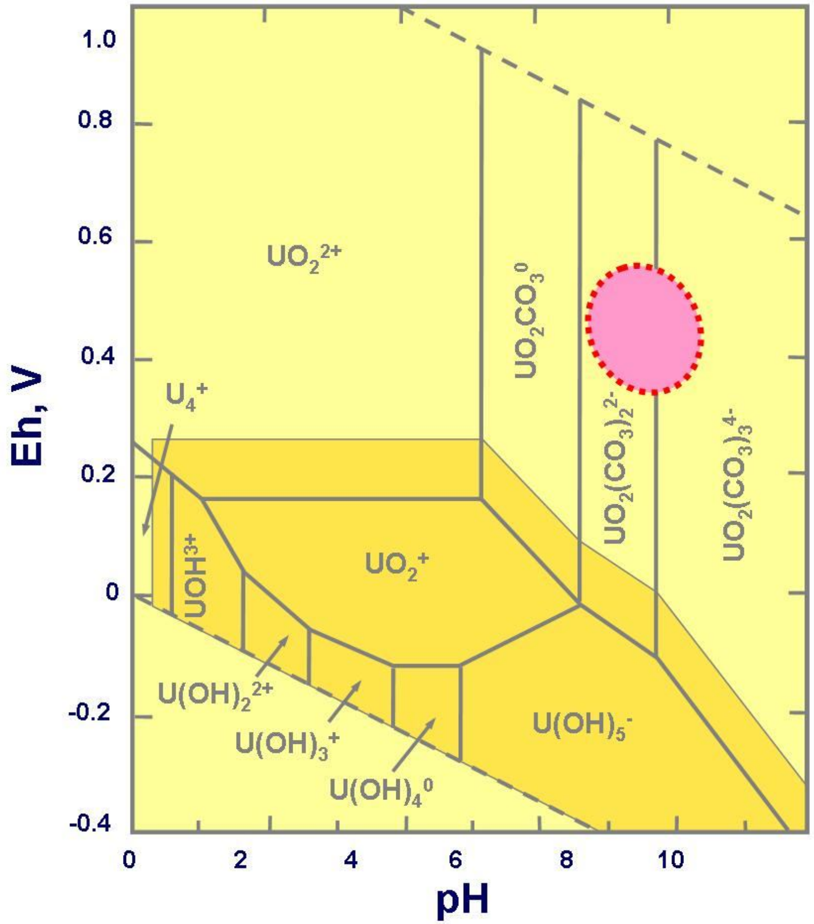

Eh-pH diagram of U-O_2-H_2O-CO^2 system, $T=25^oC$, $P=1$ atm for $U=10^{-6}$ mol, $P_{CO2}=10^{-2}$ atm (*after Langmuir, 1978*).

U speciation dominated by carbonate complexes

Dynamics of Eh-pH changes for fracture water (a) and atmospheric precipitates (b) of the TOP during 2002-2015

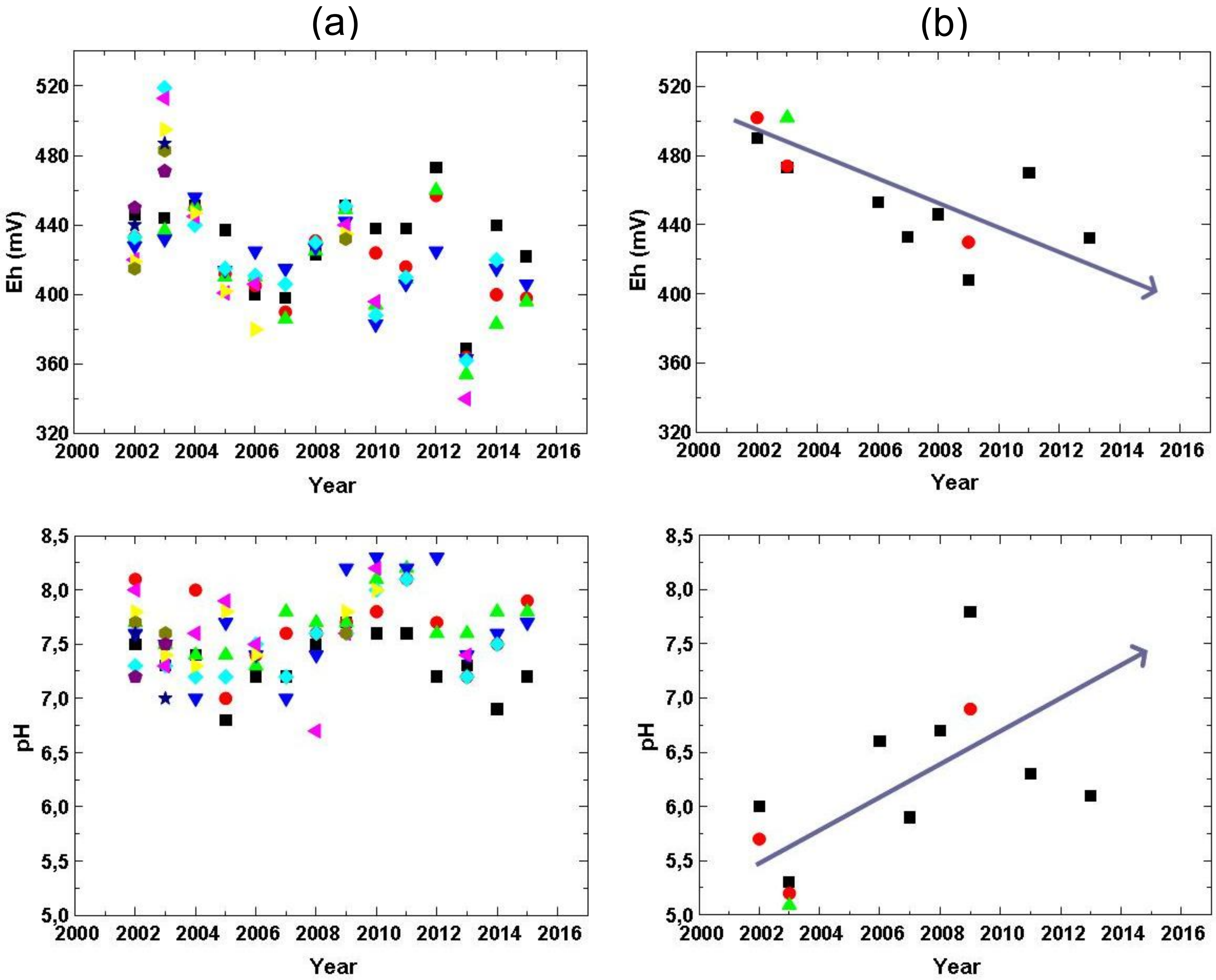

Variation of the major constituents in water sources (a) and values of δD (b) and δ18O (c) as a function of time

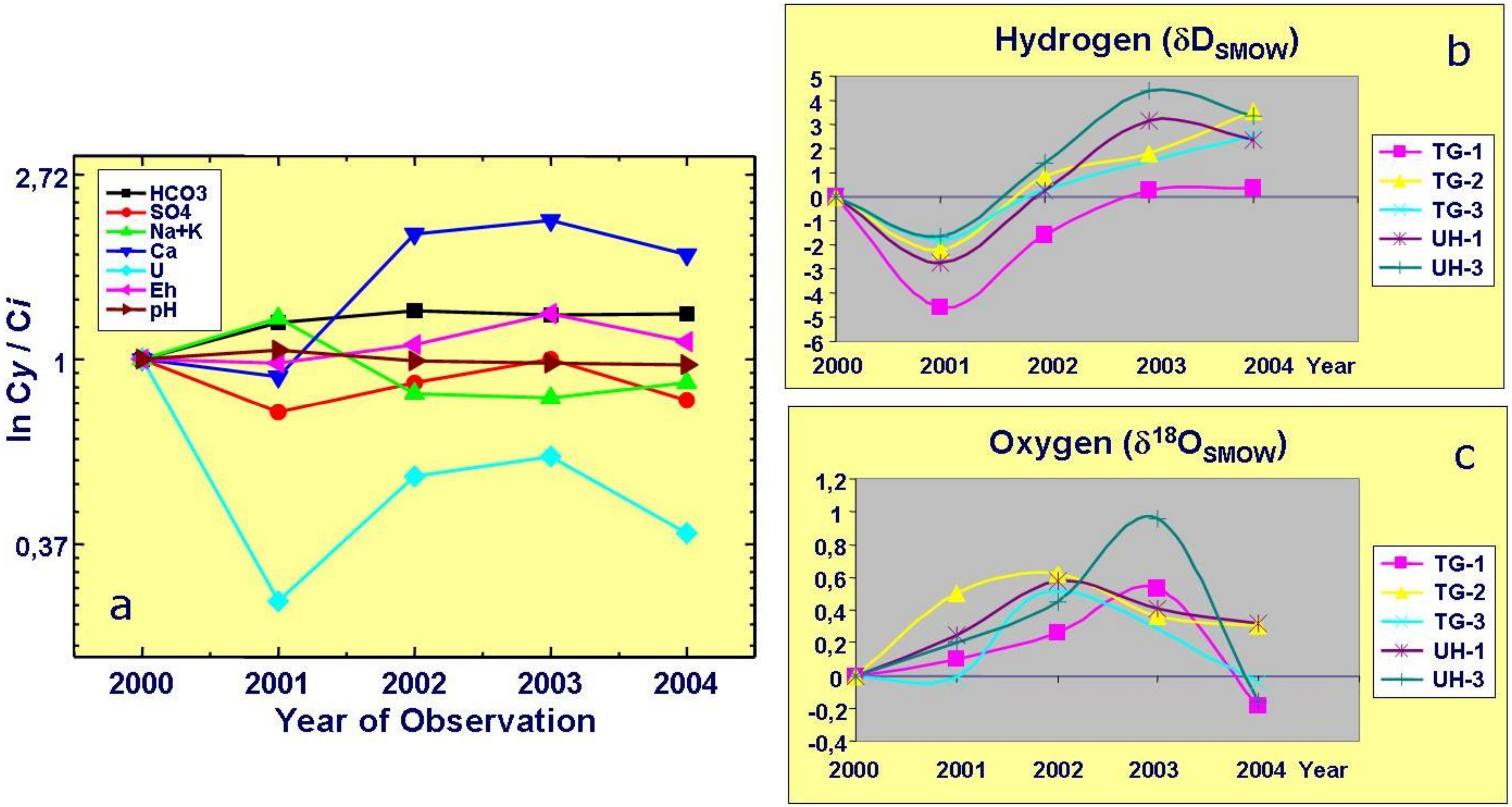

ICP-MS data on fracture water and atmospheric precipitates of the TOP

	Li	Be	V	Mn	Co	Ni	Cu	Ga	Ge	As	Se	Rb	Y	Zr
	ppb	ppb	ppb	ppb	ppb	ppb	ppb	ppb	ppb	ppb	ppb	ppb	ppb	ppb
UH1-11	371,13	0,03	1,94	43,62	0,79	1,09	2,44	1,51	0,14	37,04	1,56	7,54	0,11	0,48
UH3-11	374,23	1,57	3,55	229,06	7,11	5,69	2,70	1,35	0,15	23,77	1,74	7,51	0,64	5,08
UH4-11	362,69	0,52	3,10	189,41	2,66	4,63	4,06	2,10	0,25	26,47	1,90	10,91	2,52	28,14
TG-1-11	291,87	0,06	0,00	17,99	0,20	2,44	2,84	0,70	0,07	1,23	6,57	5,17	0,08	0,96
TG2-11	232,69	0,09	0,13	17,11	0,88	0,00	3,09	1,08	0,06	7,37	3,02	4,52	0,24	0,71
RAIN	0,62	0,03	0,39	35,71	0,22	0,00	2,27	0,86	0,03	0,41	0,00	0,67	0,29	0,04

	Cd	Sn	Sb	Te	Cs	Ba	La	Dy	Hf	Ta	W	Re	Tl	Pb
	ppb	ppb	ppb	ppb	ppb	ppb	ppb	ppb	ppb	ppb	ppb	ppb	ppb	ppb
UH1-11	3,00	0,00	17,79	0,02	37,71	81,58	0,29	0,04	0,01	0,00	0,63	0,28	0,68	4,43
UH3-11	3,31	0,00	18,59	0,02	42,70	67,28	0,75	0,17	0,11	0,01	0,70	0,28	0,34	4,85
UH4-11	4,16	0,00	24,55	0,03	42,36	106,55	1,56	0,63	0,41	0,15	0,92	0,30	0,70	13,01
TG-1-11	0,44	0,00	4,85	0,07	30,91	41,24	0,11	0,01	0,02	0,01	0,00	0,19	0,06	2,60
TG2-11	0,75	0,00	8,21	0,02	23,22	59,70	0,17	0,03	0,01	0,02	0,00	0,18	0,24	2,10
RAIN	0,40	0,00	0,00	0,00	0,03	40,95	0,37	0,08	0,01	0,01	0,05	0,00	0,01	3,05

U ore formation, modification and redeposition in the context of spatial-temporal changes of oxidizing/reducing conditions at the TOP

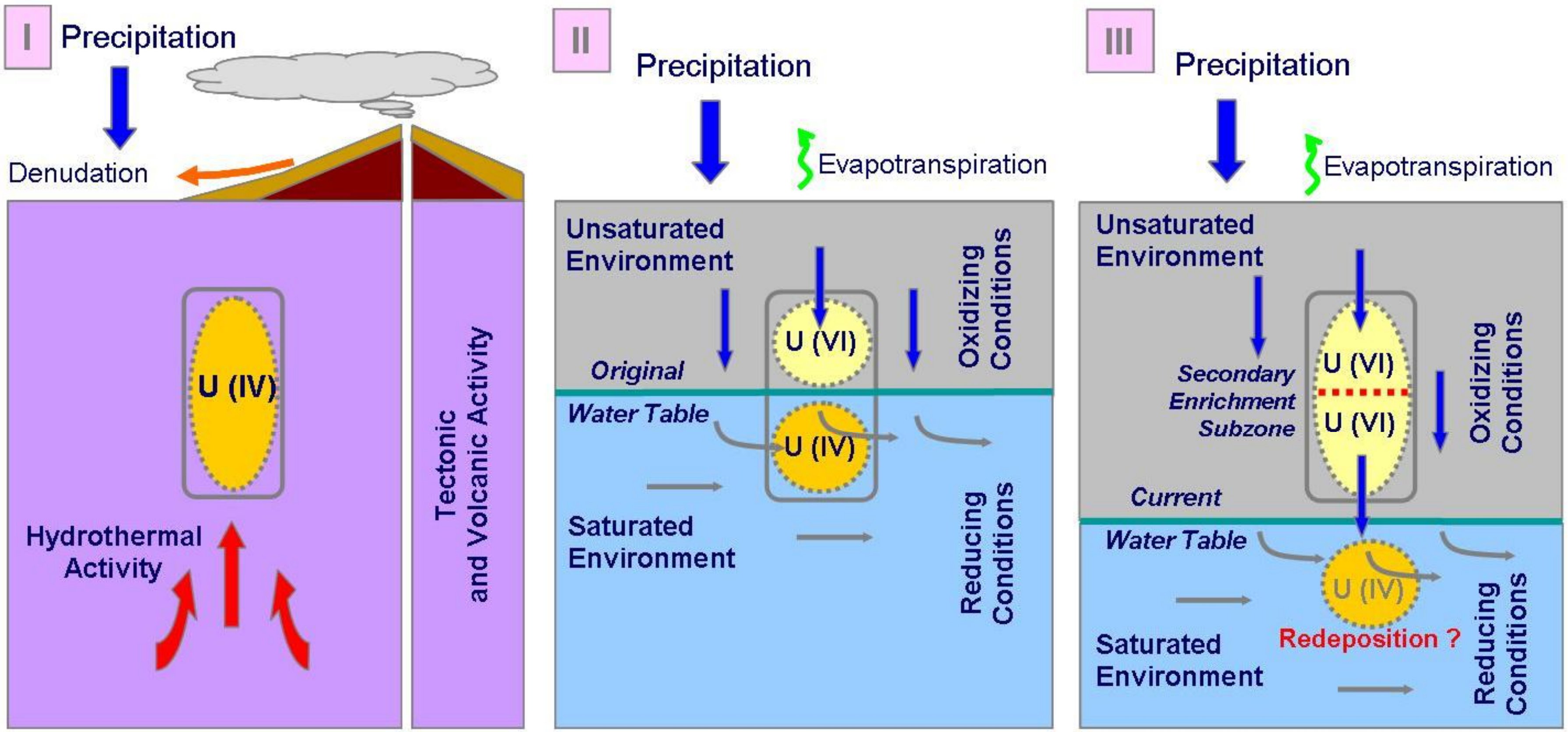

Stage of hydrothermal ore formation

Stage of the original state of the geological environment before the deposit opening

Stage of the deposit opening by an open pit, recession of water table, U transport and redeposition

Conceptual model of the redox front penetration through the fractured porous rock at oxidizing conditions

To study the conditions for U migration and accumulation in fractured porous environment

To develop and validate conceptual and numerical models for actinide migration under oxidizing conditions in unsaturated fractured rock

To provide a better understanding of actinide migration in rocks similar to SNF repositories in post-closure period

To develop PRB issues

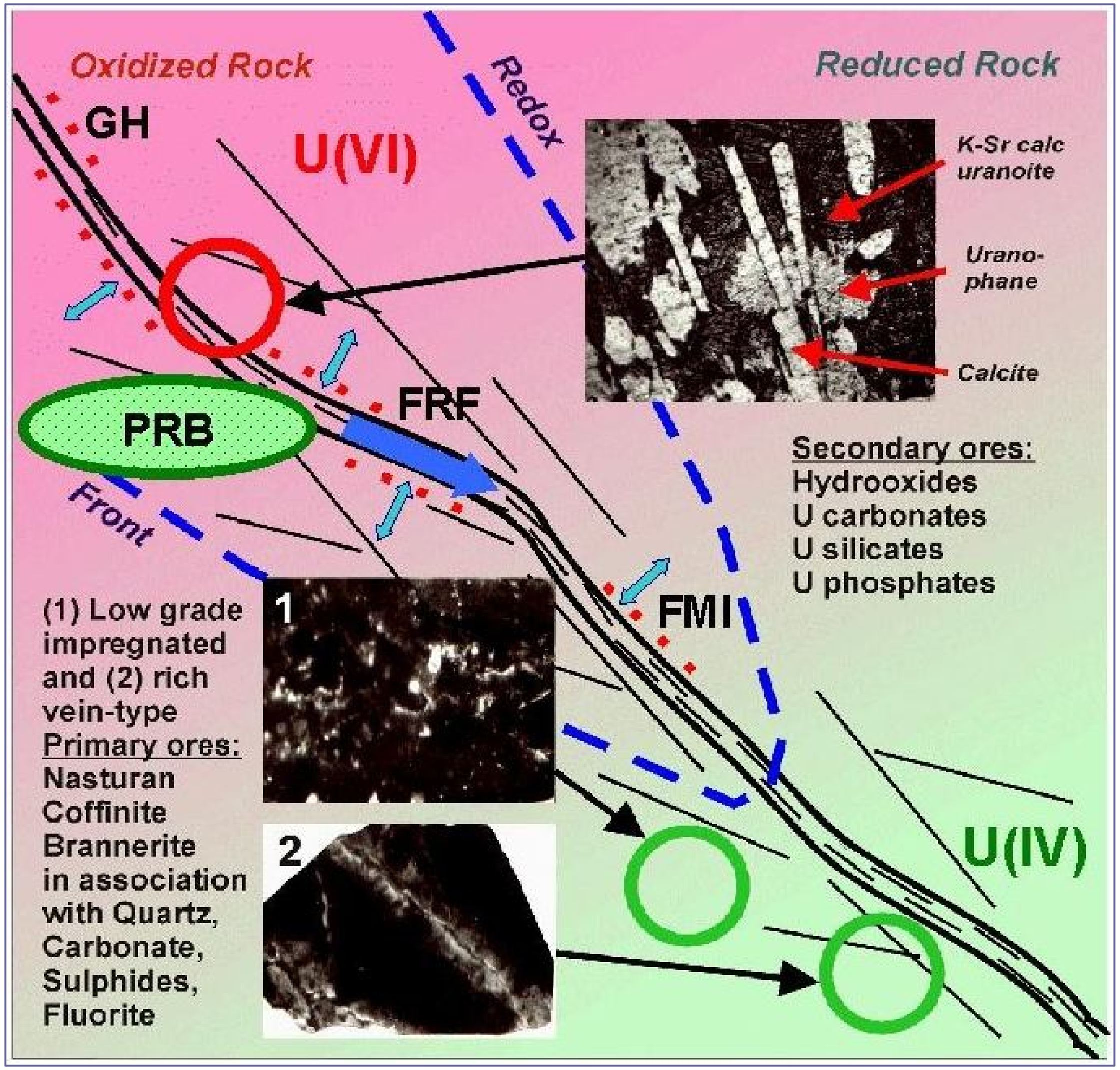

FRF - fracture reactive flow, FMI - fracture / matrix interaction, GH - goethite and hematite in the matrix bordering fluid conductive fracture, PRB - permeable reactive barrier with U-sorbing material

Mineralogical input data and Quasi-Stationary State Approximation approach (*by Lichtner, 1988*) to calculate the oxidizing front evolution

Mean mineral composition, size of mineral grains and their volumes for relatively fresh and altered rocks

Minerals	Unaltered tuff		Altered tuff	
	Volume, %	Grain size, mm	Volume, %	Grain size, mm
Oligoclase	37.5	1.5		
Albite			10.05*	1.5
Quartz	18.8	1	10.05*	1
K-feldspar	33	2	13.7*	2
Biotite	3.8	0.5		
Calcite			15.5	0.2
Ankerite			7.3	0.05
Siderite			7.3	0.05
Illite			6.3	0.005
Illite-smectite			9	0.002
Chlorite			3.7	0.01
Smectite			1.4	0.001
Kaolinite			1.8	0.005
Hematite+LA	0.9	0.001	2.7	0.001
Goethite			0.9	0.0005
Fluorite			0.41	0.1
Pitchblende			0.8	0.5
Uranophane			0.09	0.002
Bulk porosity	9.7		10.5	

Notice: * - relic minerals, LA - leucoxene-like aggregate

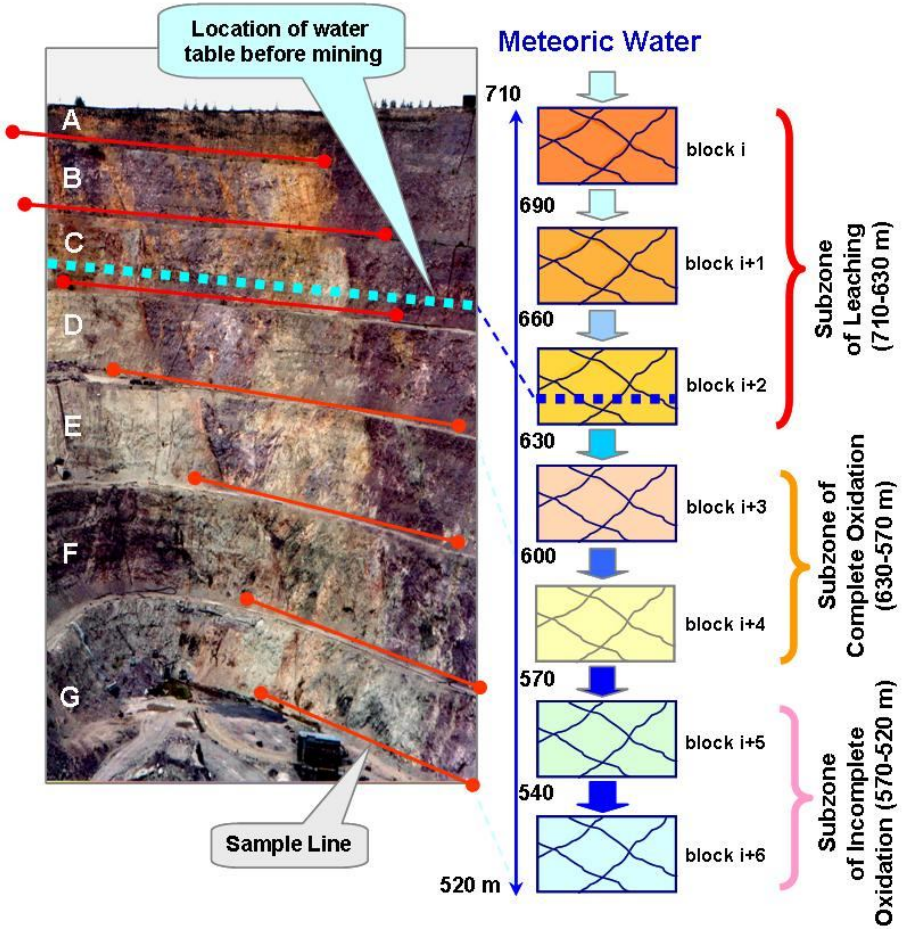

Identification of space and time relations between geochemical events, which have occurred in the vadose zone of the TOP, can be effected with a help of QSSA. For this purpose it is considered to divide the investigated column of rocks into elementary volumes (block *i*, block *i*+1…, block *i*+6) through which meteoric waters infiltrate gradually. As it is proved by our studies, every elementary volume is characterized by nearly equivalent fracture network. Application of QSSA is based on the assumption that meteoric waters penetrating the rocks react with the latter during the period required for the equilibrium of the water-rock system (formation of the adequate mineral paragenesis). It correlates with the stationary state in the elementary volume. Every stationary state is characterized by its initial mineral-chemical composition of rocks (which changes in the process of its interaction with fluid), composition of waters (which changes with the fluid infiltration from one volume to another) and rates of reacting minerals as a function of the distance.

Conceptual model of fracture density and mineral zoning for meteoric water percolation and single / double-porosity approaches of fracture flow and transport calculations

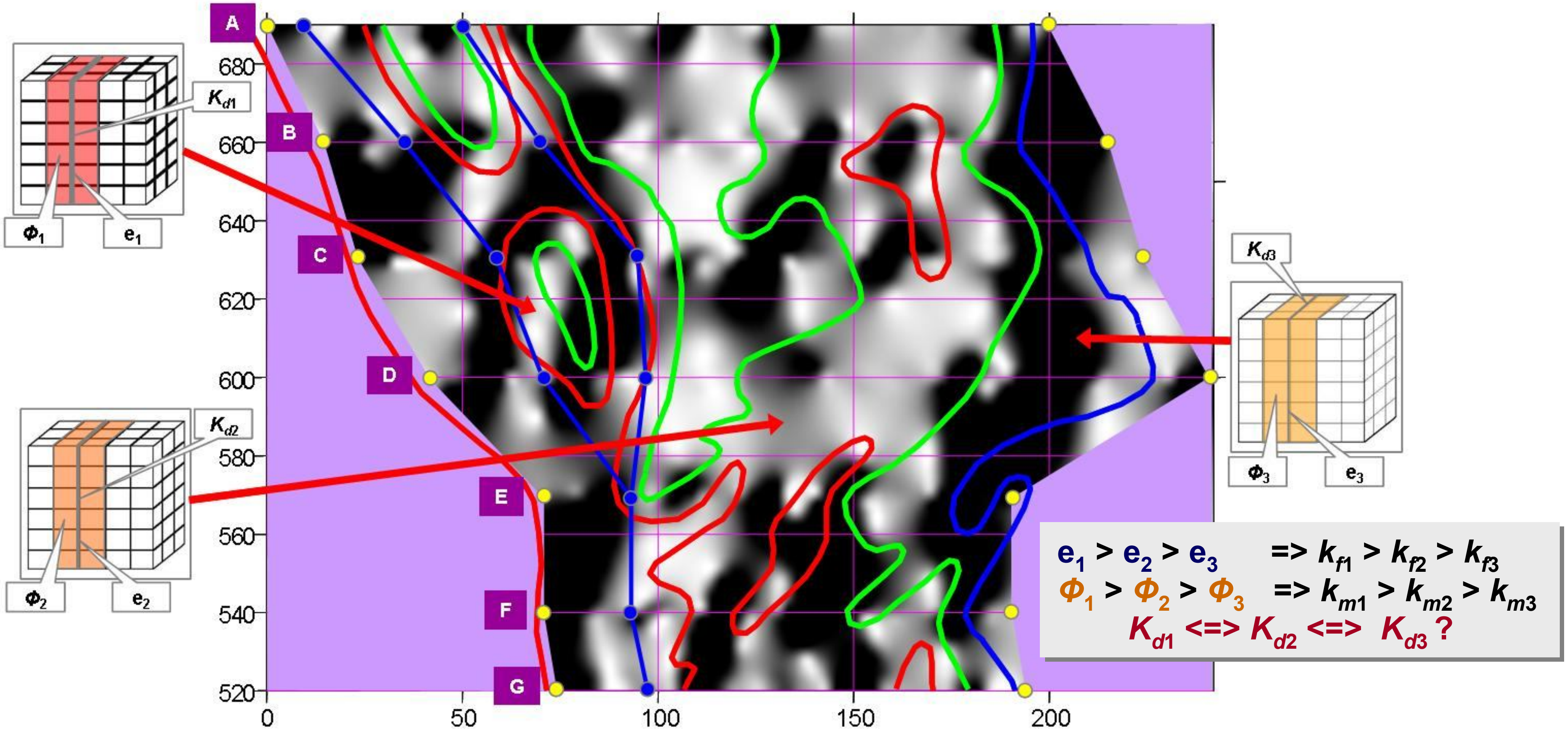

In case of substitution of the density model for aperture model then it would be possible to define the areas (2D variant) and bloks (3D variant) with specific aperture and consecutively apply the single and double-porosity models for fracture flow in unsaturated porous media. The development of the models by supplement of sorptive potential of fracture and matrix mineral fillings would be useful for a better understanding of processes of uranium migration and accumulation in the unsaturated zone of the TOP. In the figure: *e* - aperture between the fracture walls [m], *Φ* - effective porosity (dimentionless) of porous media with definite grain diameter [m], *kf* and *km* – intrinsic permeability of fracture and the rock matrix correspondingly [m^2]; *Kd* - distribution coefficient of component *k* between the liquid (water) phase and rock solids [m^3/kg].

Simplified matrix showing interrelation of U transport processes into the TOP vadose zone

Processes contributed to U retardation →

Processes contributed to U release ↓

Precipitation, Humidity, Moisture	Water/rock interactions	Redox potential (reduction)	Pore/fracture sealing	Accretion of mineral-concentrators	Durability
Changed flow conditions	**Hydrologic properties**	Reductive conditions	Pore/fracture closing, Diffusion	Positive water/mineral interaction (clay swelling)	Biomass sealing
Redox potential (oxidation), Vapor partial pressure	Oxidizing conditions	**Water chemistry**	Positive pore-water chemistry changes	Precipitation, Sorption, Altered minerals	Biomass generation, Nutrient supply, Metabolic processes
Pore/fracture ablution	Pore/fract. opening, Weakening, Coalescence flow path	Negative pore- water chemistry changes	**Pore/fracture space changes**	Positive volumetric effect, Growth of specific surface area	Positive volume changes
Leaching	Colloid transport	Mineral/water interaction, Solubility, Desorption	New surfaces	**Changes of mineral material**	Biomass accumulation, Formation of metalloorganic compounds
Biomass water consumption /releaze	Biomass dilution	Biomass microchemistry, Nutrient dilution	Biomass microfracturing, Negative volume changes	Biomass dissolution/mineralization	**Microbiotic conditions**

Summing up the obtained field and lab test data we could say that the overriding characteristic of the interactions in the vadose zone of the Tulukuevskoe Open Pit results from coupled processes.
The dominant processes can be grouped into two categories: those contributing to U release and those contributing to U retardation.
The significance and magnitude of the coupling varies both spatially and temporally.
To identify priorities, the dominant processes were considered.
The forward and back coupling of processes makes the vadose zone an environment typified by interrelated interactions.
This idea can be shown conceptually by using an interaction matrix of the type proposed by **Hudson** (1989) and developed by **Wilder** (1997).

Conclusion

- Wide range of issues related to better understanding of actinide immobilisation is covered by mineral-chemical and isotope-geochemical studies of U transfer in-situ of geological formations.

- Natural analogue studies of features, events and processes which expected to be evolved during underground disposal of RW show significant difference in approaches and tools for understanding filtration-transport properties of rocks. In this context Antey U deposit in PZ (250 Ma) granites and Tulukuevskoe U deposits in Mesozoic (140 Ma) welded tuffs provide outstanding examples of processes governing U migration and accumulation in oxidizing-reducing fracture porous environment.

- The environment reguire specific conceptual and numerical treatments because both the fractures and porous matrix are active parts of the flow and transport regimes during U transfer in hypogene and hypergene conditions. For instance, the main factors affecting the modern redox front evolution and U redistribution are fault-matrix interactions and occurrence of Permeable Reactive Barriers with mainly reducing conditions within the fluid conducting faults.

- These data could be applied for developing conceptual and numerical reactive transport models in terms of deeper insight into the spatial-temporal context of actinide migration in the natural environment in application to the HLW and SNF underground disposal.

Nevertheless there are some complications

Our vision and models

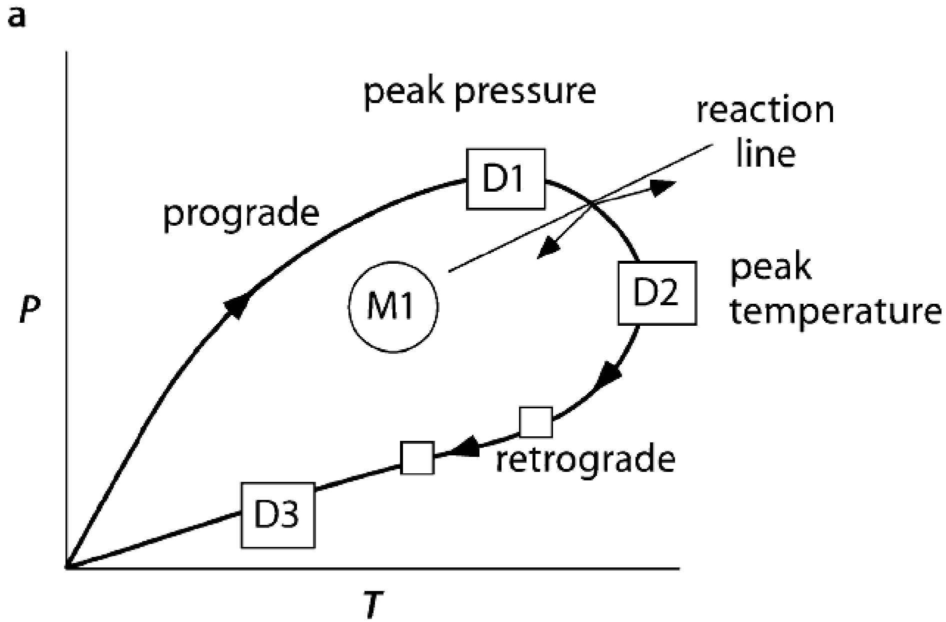

Geological reality in space and time

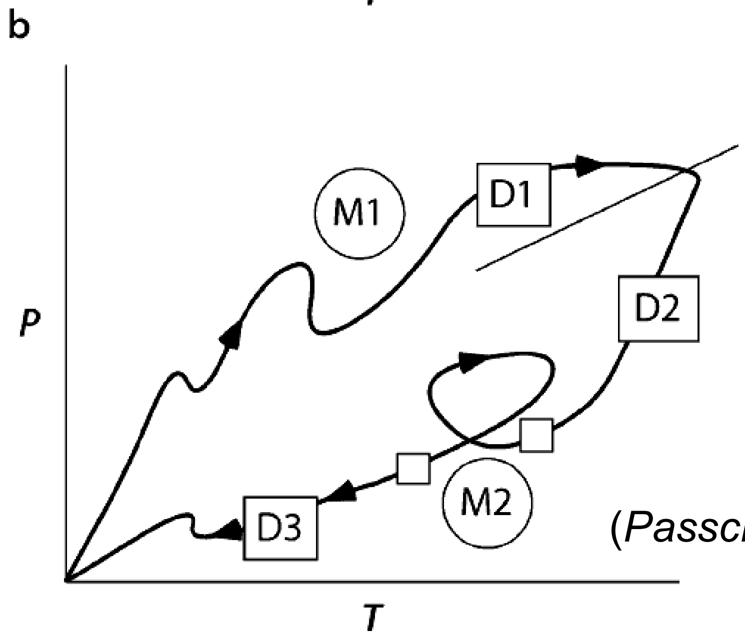

(*Passchier, Trouw, 2005*)